Framework Model For Single Proton Conduction through Gramicidin

Mark F. Schumaker,* Régis Pomès,† and Benoît Roux‡

* Department of Pure and Applied Mathematics, Washington State University, Pullman, Washington 99164-3113, USA, †Theoretical Biology and Biophysics Group, Los Alamos National Laboratory, Los Alamos, New Mexico 87545, and ‡Groupe de Recherche en Transport Membranaire, Départements de Physique et de Chimie, Université de Montréal, Québec H3C 3J7, Canada

ABSTRACT This paper describes a framework model for proton conduction through gramicidin; a model designed to incorporate information from molecular dynamics and use this to predict conductance properties. The state diagram describes both motion of an excess proton within the pore as well as the reorientation of waters within the pore in the absence of an excess proton. The model is constructed as the diffusion limit of a random walk, allowing control over the boundary behavior of trajectories. Simple assumptions about the boundary behavior are made, which allow an analytical solution for the proton current and conductance. This is compared with corresponding expressions from statistical mechanics. The random walk construction allows diffusing trajectories underlying the model to be simulated in a simple way. Details of the numerical algorithm are described.

GLOSSARY

Symbols that appear in two or more subsections are given. When uppercase and lowercase symbols are given together, lowercase denotes dimensionless quantities. Species s may represent either H (proton) or d (defect). Roman numeral R denotes either side I or side II of the channel.

Latin Symbols

a, $\hat{a}$	Weights of boundary regions. Eqs. 38, 43, and 65.
b_R	Boundary state R. See Fig. 2 *B*.
C_R, c_R	Bulk concentration on side R. See Eqs. 32 and 57.
C_0	A concentration introduced by Eq. 38; see also Eq. 72.
$C_\bullet$	The unit concentration, e.g. 1M; see Eq. 44.
$\mathscr{D}^s$	Diffusion coefficient of dipole reaction coordinate. See above Eq. 18.
d_i	Defect state i; see Fig. 2 *C*.
E	Electric field in pore interior. See above Eq. 3.
e_0	Elementary electrical charge.
f^H	Proton electrical distance. See Fig. 2 *A* and Eq. 12.
$f^d_A, f^d_B, f^d_C = f^d$	Defect electrical distances. See Fig. 2 *A* and Eqs. 13–15.
g^s	Integral defined by Eq. 120.
H_i	Proton state i; see Fig. 2 *C*.
h^s	Integral defined by Eq. 114.
i^s	Integral defined by Eq. 121.
J^s	Flux of species s; see Eq. 31.
I	Current through channel; see Eq. 83.
k_B	Boltzmann's constant.
K^s	Integration constants for P^s; see Eq. 34.
L	Spatial length of channel. See the first paragraph in Construction of the Model.
$\mathscr{L}^s$	Length of species s reaction coordinate interval. See above Eq. 18.
n	Number of random walk gridpoints for each species s. See Fig. 2 *C*.
P^s, p^s	Probability density at μ^s. See Eq. 27 and above Eq. 92.
Q^s_i	Probability that state s_i is occupied; see above Eq. 21.
Q^b_R	Probability that b_R is occupied; see above Eq. 32.
Q^H_{FW}	Framework model probability that a proton occupies the channel; Eq. 68.
Q^H_{SM}	Statistical mechanical probability of proton occupation; see Eq. 67.
T	Absolute temperature.
t^a, t^s	Access time or characteristic time for species s. See Eq. 55 and above.
V_I	Applied potential on side I; see above Eq. 3.
W^s, w^s	Total energies of species s. See Eqs. 17 and above 92.
z	Spatial coordinate coaxial with the pore. See the first paragraph in Construction of the Model.

Received for publication 14 February 2000 and in final form 2 October 2000.

Address reprint requests to Mark F. Schumaker, Washington State University, Department of Pure and Applied Mathematics, Pullman, Washington 99164. Tel.: 509-335-7273; Fax: 509-335-1188; E-mail: schumaker@wsu.edu.

Régis Pomès' present address is Structural Biology and Biochemistry, Hospital For Sick Children, Toronto, Ontario M5G 1X8, Canada.

Benoît Roux's present address is Department of Biochemistry and Structural Biology, Weill Medical College of Cornell University, 1300 York Ave., New York, New York 10021.

0006-3495/01/01/12/19 $2.00

Greek Symbols

$\alpha_R C_R$	Entrance transition probability on side *R*; see above Eq. 32.
β	$(k_B T)^{-1}$.
β_R	Exit transition probability on side *R*; see above Eq. 32.
γ_i^s	Forward transition probability from state *i*. See Fig. 2 *C* and Eq. 18.
Δt	Random walk time step; see Eq. 18.
$\Delta\tau$	Factor in Δt independent of *n*, Eq. 20.
δ_i^s	Backward transition probability from state *i*. See Fig. 2 *C* and Eq. 19.
ζ	Defined by Eq. 44.
η_R	Transition probability from b_R to interior of defect interval; see above Eq. 32.
μ^s, μ_i^s	Dipole moment reaction coordinate for species *s*. See Fig. 1 and below Eq. 17.
$\pm\mu_A^s$	Maximum extent of coordinate interval. See Fig. 1.
$\pm\mu_B^d$	Effective electrical coordinates of boundary regions. See Fig. 2 *A* and above Eq. 16.
$\pm\mu_C^d$	Maximum extent of interior of defect interval. See above Eq. 1.
ν_R	Transition probability from interior of defect interval to b_R; see above Eq. 32.
ξ^s, ξ_i^s	Dimensionless reaction coordinate for species *s*. See Eqs. 90 and 91.
Φ_B^d	See below Eq. 44.
Φ_C^d	Eq. 2.
Φ_A^H	Eq. 1.
Φ^s, ϕ^s	Potential of mean force for species *s*. See Fig. 1 and above Eqs. 1 and 92.
$\Delta\Phi^s$, $\Delta\phi^s$	Relative potentials of mean force. See Eqs. 1 and above Eq. 92.
Ψ^s, ψ^s	Applied electrostatic potential energy. See Fig. 1 and Eq. 3 and above Eq. 92.
Ψ_I, ψ_I	Energy of an elementary charge in potential V_I. See Eq. 37 and above Eq. 92.

INTRODUCTION

This paper describes the construction of a *framework* model of single proton conduction through the ion channel gramicidin. A framework model is a kinetic model, designed to incorporate potentials of mean force and diffusion coefficients computed by molecular dynamics simulations on a very short time scale, and then use this information to calculate conductances and associated observable quantities measured on a much longer time scale. The reaction coordinates of molecular dynamics simulations parameterize a simplified configuration space for the system being modeled. They explicitly parameterize the degrees of freedom thought to be most important for describing the system. But they average over fast variables; for example, those that describe intermolecular vibrations. A framework model that incorporates information from molecular dynamics is in the same sense a simplified model of configuration space.

Framework models are somewhat similar to rate theory models (reviewed by Hille, 1992), which can be regarded as zero dimensional approximations of configuration space. Rate theory models consist of states (e.g., the empty channel, an ion occupying one binding site, an ion occupying a second binding site, etc.) and transitions between them. As models of configuration space, they naturally incorporate restrictions on internal degrees of freedom due to the nature of condensed phase motion on molecular scales. For example, one may easily describe channels whose occupancy is limited to a single ion (e.g., Läuger, 1973), or multiply occupied channels (e.g., Hille and Schwarz, 1978). In this respect, rate theory models of ion permeation enjoy an important advantage over mean field models such as Goldman–Hodgkin–Katz theory (reviewed by Hille, 1992; recently used by Dieckmann et al., 1999) or Poisson-Nernst-Planck theory (for example, Chen et al., 1997; also Kurnikova et al., 1999). In these models, a probability distribution for ion concentration within the pore corresponds to an average over states of 0, 1, 2, 3, . . . ions in the pore.

Transitions between states of rate theory models are exponentially distributed in time. When these transitions describe ions within the pore, the exponential distributions can be viewed as asymptotic approximations to diffusion over energy barriers (Cooper et al., 1985, 1988). When the transitions describe ions from the bulk solution entering the pore, the exponential distribution corresponds to the assumption that the ion entry rate into an empty channel does not depend on the time elapsed since the channel last became empty (McGill and Schumaker, 1996).

However, rate theory models are not entirely satisfactory because they do not describe ion transport well when the conditions for the asymptotic approximation for diffusion over a barrier are not satisfied (Levitt, 1986; Dani and Levitt, 1990). A way to overcome this difficulty is found in the work of Levitt (1986), who showed how occupancy restrictions can be incorporated into diffusion models. McGill and Schumaker (1996) demonstrated that Levitt's model can be viewed as a diffusion within a state diagram analogous to rate theory. The diagram is parameterized by a single continuous reaction coordinate. Those authors further showed how Levitt's boundary conditions can be modified so that diffusers entering the pore are exponentially distributed in time, corresponding to ions entering an empty channel at steady state.

The framework model we construct below is designed to incorporate the molecular dynamics results of Pomès and Roux (1996, 1997, and manuscript in preparation), who show how proton permeation may be dependent on both the potential of mean force of an excess proton within the permeation pore and the potential of mean force of water

reorientation in the empty pore (that is, without an excess proton). In the first section, we construct the model as the diffusion limit of a random walk. The purpose of this construction is to obtain boundary conditions that restrict pore occupancy to a single excess charge, or a single defect in water orientation. The diffusion limit of a random walk is very well known in both the physical (Chandrasekhar, 1943) and mathematical literature (e.g., Karlin and Taylor, 1981). A good introduction can be found in the first chapter of Zauderer (1989). However, our discussion is self-contained. The boundary conditions we obtain allow the resulting model to be solved analytically.

The model is then solved for the special case of thermodynamic equilibrium, showing how the occupation probability of the pore is related to the corresponding expression from statistical mechanics. We obtain the general solution for the current through the framework model and discuss several of its properties. The solution depends on potentials of mean force and diffusion coefficients, which can be obtained from molecular dynamics. We further obtain the solution for the channel conductance, with the derivative of current with respect to applied voltage evaluated at thermodynamic equilibrium. Finally, we describe the method of numerically simulating trajectories underlying the framework model. Schumaker et al. (2000) incorporate into the framework model the results of the molecular dynamics simulations of Pomès and Roux (manuscript in preparation). They then make a detailed comparison with experiment.

CONSTRUCTION OF THE MODEL

Figure 1 *A* shows a state diagram for the dynamics of proton permeation through gramicidin based on the results of Pomès and Roux (manuscript in preparation). The state diagram consists of two segments. The top segment corresponds to diffusion of an excess proton through the pore. For simplicity, we will sometimes refer to these states as a *proton occupying the pore.* The excess proton cannot be uniquely identified. Pomès and Roux used as their reaction coordinate the axial component of the orientation moment of the pore contents. Schumaker et al. (2000) show how this may be rescaled to give the axial component of the dipole moment of the pore contents computed with respect to an origin at the center of the channel; we denote this quantity μ^{H}. To illustrate the meaning of μ^{H}, consider a simple example. Let z be the spatial coordinate co-axial with the pore, extending over the interval $-L/2 \le z \le L/2$. If we ignore pore waters and consider only an occupying proton, then $-e_0L/2 \le \mu^{\mathrm{H}} \le e_0L/2$.

The proton segment in Fig. 1 *A* is parameterized by μ^{H}, with values ranging over the interval $[-\mu_{\mathrm{A}}^{\mathrm{H}}, \mu_{\mathrm{A}}^{\mathrm{H}}]$. The value $\mu^{\mathrm{H}} = -\mu_{\mathrm{A}}^{\mathrm{H}}$ corresponds to a proton at the channel entrance on the left (side I), and $\mu^{\mathrm{H}} = \mu_{\mathrm{A}}^{\mathrm{H}}$ corresponds to a proton at the channel entrance on the right (side II). In general, we expect $\mu_{\mathrm{A}}^{\mathrm{H}} < e_0L/2$, since the polarization of the pore waters in response to the excess charge will reduce the dipole moment (Roux and Karplus, 1993). The cartoons at the upper right and left hand corners of the diagram depict states on the proton segment.

Figure 1 *B* shows the intrinsic potential of mean force, Φ^{H}, computed for the proton reaction coordinate (Pomès and Roux, 1997, and manuscript in preparation). The simulated system included the channel, pore waters, and a few waters clustered outside each channel entrance. The membrane lipid and bulk aqueous solution were not simulated. The word *intrinsic* (Levitt, 1986) refers to components of the potential apart from that due to the experimentally applied transmembrane potential. Φ^{H} has a shallow potential minimum near the center of the interval, corresponding to the excess charge located near the center of the pore.

The bottom segment of Fig. 1 *A* is parameterized by the dipole moment of the water molecules in the pore in the absence of an excess proton, denoted μ^{d}. For simplicity, we will sometimes refer to these states as corresponding to an *empty pore* or a *defect occupying the pore,* and we will refer to the bottom segment as the defect segment. Values of μ^{d} range over the interval $[-\mu_{\mathrm{A}}^{\mathrm{d}}, \mu_{\mathrm{A}}^{\mathrm{d}}]$. The value $\mu^{\mathrm{d}} = -\mu_{\mathrm{A}}^{\mathrm{d}}$ corresponds to water dipole aligned with oxygens pointing to the right and $\mu^{\mathrm{d}} = \mu_{\mathrm{A}}^{\mathrm{d}}$ corresponds to water dipoles aligned with oxygens pointing to the left.

The molecular dynamics simulations suggest that diffusion of this reaction coordinate is often associated with an *entrance-initiated* defect in the hydrogen bond chain, with water dipoles aligned on either side as suggested by the cartoons below the defect segment. This terminology was introduced by Phillips et al. (1999), and refers to a defect that originates on the side of the channel opposite an exiting proton. Those authors have suggested that defects may be exit-initiated instead. Formally, the single proton conduction model that we develop here does not depend on this choice.

Figure 1 *C* shows the intrinsic potential of mean force, Φ^{d}, computed for the defect reaction coordinate. Note that values on the abscissa increase from right to left. The potential minima are reflected in the molecular dynamics simulations by defects frequently found near one of the channel entrances, as indicated by the cartoons at the lower left and lower right of Fig. 1 *A*. These results suggest that a proton may enter a channel that has μ^{d} in a range of values concentrated near one of the potential minima. This set of possible transitions is suggested by the dashed lines between the segments in Fig. 1 *A*.

Figure 2 *A* again shows the state diagram corresponding to the dynamics of proton permeation, with the set of possible transitions between segments denoted by dashed lines. These divide the defect segment into 3 regions; compare with Fig. 1 *C*. The interior, corresponding to most of the central barrier, occupies the interval $[-\mu_{\mathrm{C}}^{\mathrm{d}}, \mu_{\mathrm{C}}^{\mathrm{d}}]$. Surrounding this are boundary region I to the left and boundary

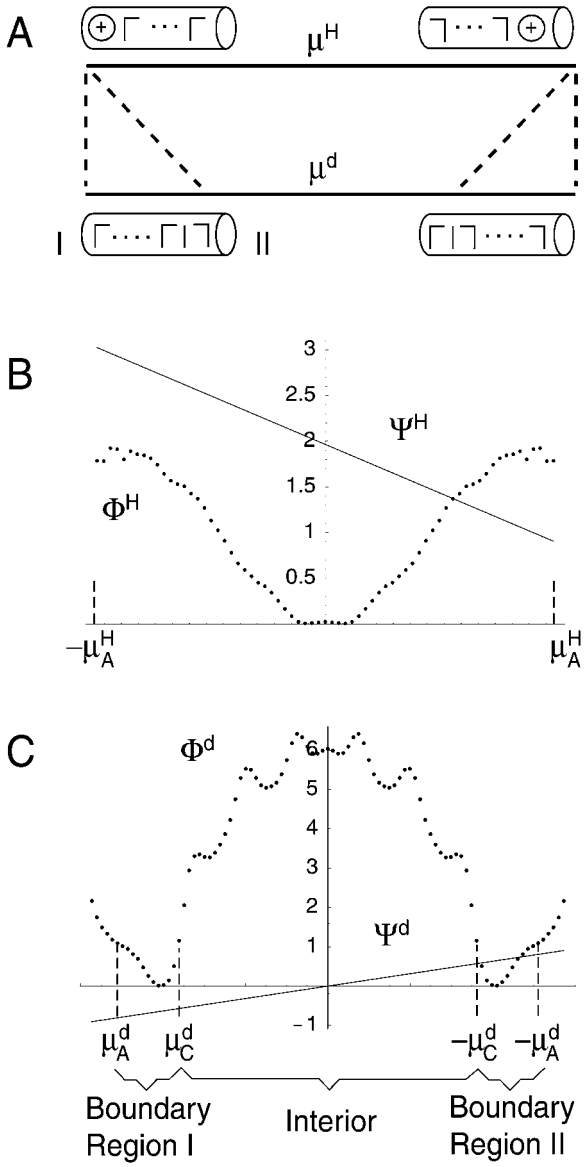

FIGURE 1 Hypothetical proton conduction mechanism. All energies are in units of k_BT for $T = 298$ K. (*A*) State diagram for proton conduction mechanism. The top segment is parameterized by the proton reaction coordinate, μ^H. Cartoons at upper left and upper right depict pore contents at the ends of the segment. An excess proton may enter from side I, at the left, and pass through the pore to exit on side II, at the right. Pore waters are depicted as angles with oxygen at the vertex. Oxygens tend to align toward the proton. The bottom segment is parameterized by the defect reaction coordinate, μ^d. A defect in the hydrogen bonding structure between waters must pass through the channel so that waters are realigned to accept another proton from side I. Dashed lines indicate that the transition from the proton-occupied state to the defect state may occur for the defect in a range of locations. (*B*) Proton potential of mean force, Φ^H (*dots*), and applied potential energy, Ψ^H (*solid*). The proton PMF shown is that calculated by Pomès and Roux (1997). Potentials are defined in the interval $-\mu_A^H < \mu^H < \mu_A^H$. (*C*) Defect PMF, Φ^d (*dots*), as calculated by Pomès and Roux (1997, and manuscript in preparation) and applied potential energy, Ψ^d (*solid*). Energy minima at either end of the central barrier correspond to a state with a defect near one end of the pore. Intervals of reaction coordinate between dashed lines on either side of the central barrier are the boundary regions. These are lumped together to form the boundary states b_I and b_{II}, shown in Fig. 2 *B*.

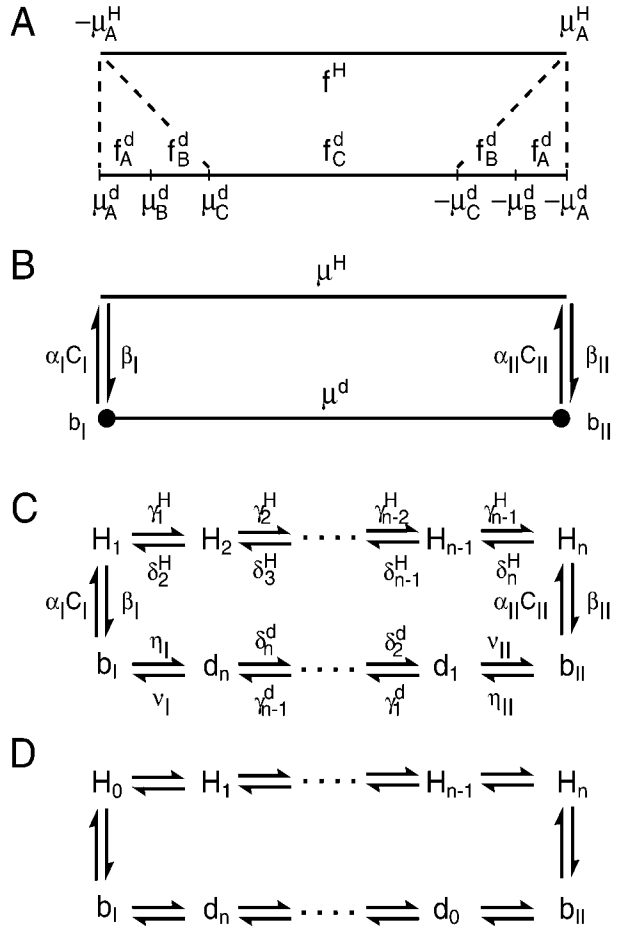

FIGURE 2 State diagrams and random walks. (*A*) State diagram of hypothetical proton conduction mechanism; compare with Fig. 1 *A*. $\pm\mu_A^H$ and $\pm\mu_A^d$ are the extreme values of the reaction coordinate intervals; compare with Fig. 1, *B* and *C*. The interior of the defect interval is bounded by coordinates $\pm\mu_C^d$. Boundary regions are the subintervals $\mu_C^d < |\mu^d| < \mu_A^d$. In the framework model they have effective electrical coordinates $\pm\mu_B^d$. The symbols f^H and f_A^d, f_B^d, and f_C^d denote the electrical width of their respective subintervals. (*B*) State diagram of the framework model. The boundary regions are lumped into boundary states b_I and b_{II}. (*C*) Random walk used to construct the framework model. States $H_1, \ldots, H_n$ scale to the proton segment in the diffusion limit, $n \to \infty$. States $d_1, \ldots, d_n$ are ordered right to left and scale to the defect segment. States b_I and b_{II} scale to the discrete boundary states. (*D*) Symmetrized random walk used by the numerical simulations. The notation for transition probabilities is similar to that shown in panel *C*.

region II to the right. Region I is the interval of defect reaction coordinate from which a proton can enter the channel on side I, and region II is the corresponding interval on side II.

The gramicidin dimer is physically symmetrical about the center of the pore, and the intrinsic potentials calculated by the molecular dynamics simulations are very nearly symmetrical about the midpoints $\mu^s = 0$, $s \in \{H, d\}$. We will assume that these potentials are exactly symmetrical. Further, there is an unknown energy difference between the

proton and defect potentials of mean force shown in Fig. 1, *B* and *C*. For these reasons, we will sometimes find it useful to refer to the following relative potentials of mean force,

$$\Delta\Phi^{H}(\mu^{H}) = \Phi^{H}(\mu^{H}) - \Phi^{H}_{A}, \quad (1)$$

$$\Delta\Phi^{d}(\mu^{d}) = \Phi^{d}(\mu^{d}) - \Phi^{d}_{C}, \quad (2)$$

where $\Phi^{H}_{A} = \Phi^{H}(\mu^{H}_{A}) = \Phi^{H}(-\mu^{H}_{A})$, and $\Phi^{d}_{C} = \Phi^{d}(\mu^{d}_{C}) = \Phi^{d}(-\mu^{d}_{C})$.

Applied Field

Let $V(z)$ denote the component of the electrostatic potential due to an applied transmembrane potential, V_I, on side I. It is independent of the charge distribution of the channel and the pore waters (Roux, 1997). $V(z)$ is assumed to drop linearly over the length of the channel, corresponding to a constant electric field $E = V_I/L$ in the positive z direction. This form for the potential is appropriate for the simple cylindrical geometry of gramicidin (Jordan et al., 1989; Roux, 1999). Some feathering of the potential does occur near the channel entrances in these calculations, but, for simplicity, we will use the linear approximation.

When the applied electric field is constant, the resulting contribution to the potential energy of the pore contents depends only on its net charge and dipole moment (e.g., Jackson, 1975). This is seen by considering the electrical potential energy, Ψ^{s}, as a function of the charge density, $\rho^{s}(z)$, associated with species s and the electrical potential $V(z)$,

$$\Psi^{s} = \int_{-L/2}^{L/2} \rho^{s}(z)V(z)\,dz, \quad (3)$$

where the electrical potential is given by the linear drop

$$V(z) = V_I/2 - zE \quad (4)$$

over the interval $-L/2 < z < L/2$. For the cases of the proton occupied and empty pores, the applied potential energy can be written in the forms,

$$\Psi^{H} = e_0V_I/2 - \mu^{H}E, \quad (5)$$

$$\Psi^{d} = -\mu^{d}E, \quad (6)$$

where e_0 is the elementary electronic charge, and μ^{s} is the dipole moment reaction coordinate. Electrical potential energies corresponding to $V_I = 0.1$ V are shown in Fig. 1, *B* and *C*.

The potential energy drop around the cycle of the state diagram in Fig. 2 *A* must be zero. To compute the drop, consider the following energy differences:

$$\Psi^{H}(-\mu^{H}_{A}) - \Psi^{H}(\mu^{H}_{A}) = 2\mu^{H}_{A}E, \quad (7)$$

$$\Psi^{H}(\mu^{H}_{A}) - \Psi^{d}(-\mu^{d}_{A}) = 0, \quad (8)$$

$$\Psi^{d}(-\mu^{d}_{A}) - \Psi^{d}(\mu^{d}_{A}) = 2\mu^{d}_{A}E, \quad (9)$$

$$\Psi^{d}(\mu^{d}_{A}) - \Psi^{H}(-\mu^{H}_{A}) = -e_0V_I, \quad (10)$$

Eqs. 7 and 9 follow directly from Eqs. 5 and 6. To verify Eq. 8, consider a proton leaving the channel at $\mu^{H} = \mu^{H}_{A}$ on side II. We assume that the orientation of the water dipoles in this state and the state $\mu^{d} = -\mu^{d}_{A}$ are the same. Because the electrical potential energy of the proton on side II is zero, it then follows that $\Psi^{H}(\mu^{H}_{A})$ and $\Psi^{d}(-\mu^{d}_{A})$ are equal. Similarly, Eq. 10 is obtained by considering that a proton leaving the channel from side I carries with it a potential energy e_0V_I. Adding Eqs. 7–10 and dividing by E gives

$$2\mu^{H}_{A} + 2\mu^{d}_{A} = e_0L. \quad (11)$$

This equation relates the physical length of the pore with the maximum values of the proton and defect reaction coordinates. When the values μ^{H}_{A} and μ^{d}_{A} obtained from the molecular dynamics simulations of Pomès and Roux (manuscript in preparation) are used, we obtain the result $L = 22.9$ Å (Schumaker et al., 2000). This is slightly shorter than the physical length of the pore. The discrepancy may be due to the confinement of the excess proton in the molecular dynamics simulations (Schumaker et al., 2000).

It is convenient to introduce dimensionless electrical distances, analogous to those encountered in rate theory (e.g., Hille, 1992).

$$f^{H} = 2\mu^{H}_{A}/(e_0L), \quad (12)$$

$$f^{d}_{A} = (\mu^{d}_{A} - \mu^{d}_{B})/(e_0L), \quad (13)$$

$$f^{d}_{B} = (\mu^{d}_{B} - \mu^{d}_{C})/(e_0L), \quad (14)$$

$$f^{d} = f^{d}_{C} = 2\mu^{d}_{C}/(e_0L), \quad (15)$$

where the notation f^{d} is used in the appendices. These electrical distances are proportional to widths of subintervals of reaction coordinate as shown in Fig. 2 *A*. Eqs. 13 and 14 refer to the value μ^{d}_{B}. The points $\mu^{d} = \pm\,\mu^{d}_{B}$ are shown in Fig. 2 *A* and will be the effective electrical coordinates of the boundary regions. Expressing Eq. 11 in terms of the electrical distances, we have

$$2f^{d}_{A} + 2f^{d}_{B} + f^{d}_{C} + f^{H} = 1. \quad (16)$$

The total energy, W, of the pore contents is the sum of the intrinsic and applied potentials,

$$W^{s}(\mu^{s}) = \Phi^{s}(\mu^{s}) + \mu_{s}(\mu_{s}). \quad (17)$$

Random walk limit to a diffusion process

In this section, we construct the framework model for proton diffusion through gramicidin, whose state diagram is shown in Fig. 2 *B*. The random walk construction that we use obtains the Smoluchowski equations (or their first inte-

grals, the Nernst–Planck equations), which describe diffusion of the reaction coordinates μ^H and μ^d in the proton-occupied or proton-empty channels, respectively. Most significantly, the construction also obtains the boundary conditions that make possible a description of diffusion on the state diagram, which is a simplified configuration space for proton conduction through gramicidin. That is, by the structure of the random walk, we describe either the diffusion of a single excess charge through the channel or the diffusion of the axial component of the dipole moment of the pore waters in the absence of an excess charge.

The difference between the state diagram of Fig. 2 *B* and that of Fig. 2 *A* lies in the description of the boundary regions $\mu_C^d < |\mu^d| < \mu_A^d$. The framework model lumps these into discrete boundary states b_I and b_{II} in the *lumped state approximation.* These states are constructed so that their probabilities are equal to the integral of the Boltzmann factor over the boundary regions under conditions of symmetrical equilibrium; see Eq. 64 below. This approximation greatly simplifies the mathematical description of entrance and exit. Instead of a continuum of possible transitions between the boundary regions on the defect segment and the endpoints of the proton segment, as suggested by Fig. 2 *A,* we have a pair of transitions between the lumped states b_I and b_{II} and the proton segment, shown in Fig. 2 *B.* The lumped states surround the interior of the defect segment, which contains the central barrier shown in Fig. 1 *C.* Transport of the defect reaction coordinate μ^d in the interior is described diffusively, by a Nernst–Planck equation. This lumped-state approximation gives an accurate description of transport over the barrier (Schumaker et al., 2000; Mapes and Schumaker, submitted) while leading to a model that is analytically solvable.

The state diagram of the random walk is shown in Fig. 2 *C.* It is discrete in both space and time. State H_i, $i \in \{1, 2, \ldots, n\}$, denotes a proton at coordinate $\mu_i^H = \mu_A^H(2i/n - 1)$, and state d_i, $i \in \{1, 2, \ldots, n\}$, denotes a defect at coordinate $\mu_i^d = \mu_C^d(2i/n - 1)$. State s_i will refer to either H_i or d_i. The two additional states b_I and b_{II} will be taken to the boundary states of Fig. 2 *B* by the random walk construction. There are altogether $2n + 2$ states in the random walk. We will define transition probabilities appropriately and take the limit $n \to \infty$ to obtain the framework model.

Nernst–Planck equation for channel interior

Let $\mathscr{L}^H = 2\mu_A^H$ and $\mathscr{L}^d = 2\mu_C^d$ be the lengths of the reaction coordinate intervals over which transport will be described by a diffusion process. The distance between the states s_i of Fig. 2 *C* is $\Delta\mathscr{L}^s = \mathscr{L}^s/n$. Diffusion over the reaction coordinate intervals is described by diffusion coefficients, $\mathscr{D}^s$, having units of (dipole moment)^2/time; for simplicity, we assume that these are constants, independent of μ^s.

The probabilities, γ_i^s, for a transition from state s_i to s_{i+1}, and δ_i^s, for a transition from s_i to s_{i-1}, are given by

$$\gamma_i^s = \Delta t \frac{\mathscr{D}^s}{(\Delta\mathscr{L}^s)^2} \exp\left(\frac{1}{2}\beta[W^s(\mu_i^s) - W^s(\mu_{i+1}^s)]\right), \quad (18)$$

$$\delta_i^s = \Delta t \frac{\mathscr{D}^s}{(\Delta\mathscr{L}^s)^2} \exp\left(\frac{1}{2}\beta[W^s(\mu_i^s) - W^s(\mu_{i-1}^s)]\right), \quad (19)$$

where $\beta = (k_B T)^{-1}$ and Δt is the time interval between steps of this discrete-time random walk. We scale Δt with n so that the leading order of n in the expressions for γ_i^s and δ_i^s is n^0; transition probabilities then remain positive and finite in the limit $n \to \infty$. Let

$$\Delta t = \Delta\tau/n^2, \quad (20)$$

where $\Delta\tau$ is independent of n. $\Delta\tau$ must be chosen so that the probability of leaving a state at each time step is no greater than 1. This choice is made explicitly by the algorithm described in Numerical Solution below.

The transition probabilities γ_i^s and δ_i^s lead to the Boltzmann distribution at equilibrium. To see this, let Q_i^s be the probability that state s_i of the random walk is occupied. At equilibrium, the system is in detailed balance with zero net flux between any two states. This means

$$Q_i^s \gamma_i^s = Q_{i+1}^s \delta_{i+1}^s . \quad (21)$$

Inserting the definitions for the transition probabilities gives the result expected from the Boltzmann distribution,

$$Q_i^s/Q_{i+1}^s = \exp \beta[W^s(\mu_{i+1}^s) - W^s(\mu_i^s)]. \quad (22)$$

The transition probabilities may be expanded in the small parameter $1/n$ to give a useful expression in preparation for taking the limit $n \to \infty$. The expansion gives

$$\gamma_i^s = \Delta t \frac{\mathscr{D}^s}{(\Delta\mathscr{L}^s)^2}\left\{1 - \frac{1}{2}\beta\Delta\mathscr{L}^s W^{s\prime}(\mu_i^s) + (\Delta\mathscr{L}^s)^2\epsilon_i^s + \mathbb{O}(n^{-3})\right\}, \quad (23)$$

$$\delta_i^s = \Delta t \frac{\mathscr{D}^s}{(\Delta\mathscr{L}^s)^2}\left\{1 + \frac{1}{2}\beta\Delta\mathscr{L}^s W^{s\prime}(\mu_i^s) + (\Delta\mathscr{L}^s)^2\epsilon_i^s + \mathbb{O}(n^{-3})\right\}, \quad (24)$$

where

$$\epsilon_i^s = -\beta W^{s\prime\prime}(\mu_i^s)/4 + \beta^2 W^{s\prime}(\mu_i^s)^2/8, \quad (25)$$

and primes denote derivatives with respect to the argument. We assume $W^{s\prime\prime}$ is continuous. The transition probabilities used by McGill and Schumaker (1996) are obtained from Eqs. 23 and 24 by truncating after the first-order terms.

We now construct a limit of the random walk that leads to the Nernst–Planck equation at steady state. Consider the

states s_i, $2 \le i \le n-1$. At steady state, the total probability flowing into s_i at each time step equals the total probability flowing out. Equating these flows, we have the expression for probability balance,

$$Q_i^s(\gamma_i^s + \delta_i^s) = Q_{i+1}^s \delta_{i+1}^s + Q_{i-1}^s \gamma_{i-1}^s . \tag{26}$$

Each state, s_i, represents a segment of the s interval of length $\Delta\mathcal{L}^s = \mathcal{L}^s/n$. While taking the limit $n \to \infty$, we wish to consider the density, P^s, related to the state probabilities by

$$Q_i^s = P_i^s \Delta\mathcal{L}^s, \quad \text{where} \quad P_i^s = P^s(\mu_i^s). \tag{27}$$

Substitute Eqs. 23, 24, and 27 into 26, simplify, and use the following finite difference expressions for first and second derivatives:

$$(W^{s\prime}(\mu^s)P^s(\mu^s))' = \lim_{n\to\infty} (W_{i+1}^{s\prime} P_{i+1}^s - W_{i-1}^{s\prime} P_{i-1}^s)/(2\Delta\mathcal{L}^s), \tag{28}$$

$$P^{s\prime\prime}(\mu^s) = \lim_{n\to\infty} (P_{i+1}^s - 2P_i^s + P_{i-1}^s)/(\Delta\mathcal{L}^s)^2, \tag{29}$$

where $W_i^{s\prime} = W^{s\prime}(\mu_i^s)$ and $\mu_i^s \to \mu^s$ as $n \to \infty$. Note from Eq. 25 that ϵ_i^s tends to a continuous function of μ^s in this limit. We obtain the Smoluchowski equation,

$$0 = \frac{d^2P^s}{d(\mu^s)^2} + \frac{d}{d\mu^s}\beta W'(\mu^s)P^s. \tag{30}$$

This is a diffusion equation with the second term corresponding to a systematic force on the diffuser whose magnitude is proportional to the gradient of the potential energy W'. Integrating once, we obtain the Nernst–Planck equation,

$$J^s = -\mathcal{D}^s\left(\frac{dP^s}{d\mu^s} + \beta W'(\mu^s)P^s\right), \tag{31}$$

where J^s is the flux of species s. The first term on the right-hand side is Fick's law, and the second term corresponds to the systematic force.

Note that J^s is positive when it is in the direction of increasing μ^s. That means that the flux of protons is positive when directed from left to right in Fig. 2 *A,* whereas the flux of defects is positive when directed from right to left. In both cases, positive flux corresponds to progress in the clockwise direction around the diagram.

Entrance and exit transition probabilities

In this subsection, we obtain expressions for the entrance and exit transition probabilities that connect the following states in Fig. 2 *C:* H_1, b_I, and d_n on side I of the pore and H_n, b_{II}, and d_1 on side II. In particular, these probabilities are scaled with n to obtain, in the limit $n \to \infty$, the state diagram of Fig. 2 *B.* In this figure, the interior of the defect segment supports a probability density and the endpoints, b_I and b_{II}, have positive probability. The limit on n is taken in the Boundary conditions subsection, following this one.

We begin the formal development by considering proton transitions into and out of the channel for the random walk state diagram shown in Fig. 2 *C.* At equilibrium, there is no net flow of ions into the channel at either entrance. On side I, we form the detailed balance relationships between H_1 and b_I and between b_I and d_n and use these to eliminate Q_I^b; the probability that boundary state b_I is occupied. Similarly, we eliminate Q_{II}^b on side II. This leads to

$$\frac{Q_1^H}{Q_n^d} = \frac{\alpha_I C_I}{\beta_I}\frac{\nu_I}{\eta_I}, \tag{32}$$

$$\frac{Q_n^H}{Q_1^d} = \frac{\alpha_{II} C_{II}}{\beta_{II}}\frac{\nu_{II}}{\eta_{II}}, \tag{33}$$

where the C_R are the excess proton concentrations on side R. We use concentrations instead of activities because diffusion coefficients are defined in terms of concentration gradients (Robinson and Stokes, 1965; see also McGill and Schumaker, 1996).

We require that the detailed balance equations remain satisfied in the limit $n \to \infty$. In this limit, Q_1^H and Q_n^H converge to values proportional to the probability density P^H on the proton segment at the endpoints $-\mu_A^H$ and $+\mu_A^H$, respectively. Similarly, Q_1^d and Q_n^d converge to values proportional to $P^d(-\mu_C^d)$ and $P^d(\mu_C^d)$, respectively. The equilibrium densities on the proton and defect segments are obtained by solving Eq. 31 with $J^s = 0$, giving the Boltzmann distribution,

$$P^s(\mu^s) = K^s e^{-\beta W^s(\mu^s)}, \tag{34}$$

where the K^s are constants. Take the limit of Eqs. 32 and 33 as $n \to \infty$, using Eqs. 27 and 34. We obtain

$$\lim_{n\to\infty} \frac{\alpha_I C_I}{\beta_I}\frac{\nu_I}{\eta_I} = \frac{K^H}{K^d}\exp(\beta[W^d(\mu_C^d) - W^H(-\mu_A^H)]), \tag{35}$$

$$\lim_{n\to\infty} \frac{\alpha_{II} C_{II}}{\beta_{II}}\frac{\nu_{II}}{\eta_{II}} = \frac{K^H}{K^d}\exp(\beta[W^d(-\mu_C^d) - W^H(\mu_A^H)]). \tag{36}$$

From the left-hand side of these equations, we see that the constant K^H/K^d must be proportional to C_I in the first of these equations and to C_{II} in the second. This may be understood by considering the Nernst equation,

$$C_{II} = C_I e^{\beta\Psi_I}, \tag{37}$$

where $\Psi_I = eV_I$. We will set

$$\frac{K^H}{K^d} = \frac{\hat{a}C_I}{\hat{a}C_0}e^{\beta\Psi_I} = \frac{\hat{a}C_{II}}{\hat{a}C_0}, \tag{38}$$

where the dimensionless quantity, $\hat{a}$, and the concentration, C_0, have been introduced. We assume these do not depend on C_I, C_{II}, or Ψ_I. Below, $\hat{a}$ is determined by the requirement

that occupation probabilities of the framework model agree with statistical mechanics in the case of a symmetrical equilibrium ($V_I = 0$). We discuss C_0 further in Equilibrium Probability for Proton Occupation.

Insert the second expression of Eq. 38 into the right-hand side of Eq. 35 and the third expression of Eq. 38 into the right-hand side of Eq. 36. The resulting detailed balance relationships are satisfied by the following decomposition

$$\lim_{n\to\infty} \frac{n\alpha_I C_I}{\beta_I} = \frac{1}{\hat{a}} \frac{C_I}{C_0} \exp(\beta[W^d(\mu_B^d) - W^H(-\mu_A^H) + \Psi_I]), \tag{39}$$

$$\lim_{n\to\infty} \frac{\nu_I}{n\eta_I} = \hat{a} \exp(\beta[W^d(\mu_C^d) - W^d(\mu_B^d)]), \tag{40}$$

$$\lim_{n\to\infty} \frac{n\alpha_{II} C_{II}}{\beta_{II}} = \frac{1}{\hat{a}} \frac{C_{II}}{C_0} \exp(\beta[W^d(-\mu_B^d) - W^H(\mu_A^H)]), \tag{41}$$

$$\lim_{n\to\infty} \frac{\nu_{II}}{n\eta_{II}} = \hat{a} \exp(\beta[W^d(-\mu_C^d) - W^d(-\mu_B^d)]). \tag{42}$$

In making this decomposition, the boundary points b_I and b_{II} are formally assigned defect reaction coordinates $\pm\mu_B^d$. The additional term Ψ_I in the exponent on the right-hand side of Eq. 39 represents the electrostatic energy of an ion entering on side I. The distribution of factors of n on the left-hand side of Eqs. 39–42 reflects the fact that the rates of transitions from the proton and defect segments into the boundary states b_I and b_{II} must scale with one power of n higher than the rates of transitions from the boundary states back to the segments. This is because the boundary state probabilities Q_I^b and Q_{II}^b remain positive in the limit $n \to \infty$ while the states s_1 and s_n, $s \in \{H, d\}$, scale to the endpoints of probability densities.

We next introduce the new quantities

$$a = \hat{a} \exp(\beta[\Phi_C^d - \Phi_B^d]), \tag{43}$$

$$\zeta = \Phi_C^d - \Phi_A^H - k_B T \ln C_0/C_\bullet, \tag{44}$$

where $\Phi_B^d = \Phi^d(\mu_B^d) = \Phi^d(-\mu_B^d)$ and $C_\bullet$ is the unit concentration, e.g., $C_\bullet = 1$ M (the argument of the logarithm must be dimensionless). In the expression for ζ, the term $\Phi_C^d - \Phi_A^H$ depends on the absolute energy difference between the proton and defect potentials of mean force. This energy difference was not determined by the molecular dynamics. As a consequence, ζ will be treated as an adjustable parameter in our analysis of the Eisenman et al. (1980) conductance data using the single proton model (Schumaker et al., 2000).

We now simplify the exponents of Eqs. 39–42 by replacing $\hat{a}$ with a, decomposing W according to Eq. 17, expressing Ψ^H in terms of Ψ^d using Eqs. 8 and 10, using the definitions for electrical distances, Eqs. 13 and 14, and finally introducing the definition of ζ. The result is

$$\lim_{n\to\infty} \frac{n\alpha_I C_I}{\beta_I} = \frac{1}{a} \frac{C_I}{C_\bullet} \exp(\beta[f_A^d \Psi_I + \zeta]), \tag{45}$$

$$\lim_{n\to\infty} \frac{\nu_I}{n\eta_I} = a \exp(\beta f_B^d \Psi_I), \tag{46}$$

$$\lim_{n\to\infty} \frac{n\alpha_{II} C_{II}}{\beta_{II}} = \frac{1}{a} \frac{C_{II}}{C_\bullet} \exp(\beta[-f_A^d \Psi_I + \zeta]), \tag{47}$$

$$\lim_{n\to\infty} \frac{\nu_{II}}{n\eta_{II}} = a \exp(-\beta f_B^d \Psi_I). \tag{48}$$

The following definitions are consistent with these constraints:

$$\alpha_I = \alpha_{II} = \Delta t (t^a)^{-1} a^{-1} C_\bullet^{-1} e^{\beta\zeta}, \tag{49}$$

$$\beta_I = \Delta t (t^a)^{-1} n \exp(-\beta f_A^d \Psi_I), \tag{50}$$

$$\beta_{II} = \Delta t (t^a)^{-1} n \exp(\beta f_A^d \Psi_I), \tag{51}$$

$$\nu_I = \Delta t (t^d)^{-1} n^2 a \exp(\beta f_B^d \Psi_I), \tag{52}$$

$$\nu_{II} = \Delta t (t^d)^{-1} n^2 a \exp(-\beta f_B^d \Psi_I), \tag{53}$$

$$\eta_I = \eta_{II} = \Delta t (t^d)^{-1} n, \tag{54}$$

where the access time, t^a, is the second free parameter optimized to fit the Eisenman et al. data set. We also introduce the proton and defect diffusion times

$$t^s = (\mathscr{L}^s)^2/\mathscr{D}^s, \tag{55}$$

where $s \in \{H, d\}$. Eqs. 49–54 complete our description of the discrete-time, discrete-state random walk whose state diagram is shown in Fig. 2 *C*. The time step is Δt. The transition probabilities $\alpha_R C_R$, β_R, ν_R, and η_R, $R \in \{I, II\}$, are all dimensionless. The rates of transitions into the proton segment, equal to $\alpha_R C_R/\Delta t$, are independent of n. The scaling of the β_R with n is then determined by the constraints given in Eqs. 45 and 47.

Our scaling of the entrance rate as independent of n means that proton entrances are exponentially distributed in time when the channel is accessible to protons. For example, when the system is near boundary state b_I of Fig. 2 *B*, one waits an exponentially distributed length of the accumulated time spent in state b_I before a proton enters the channel. This is very similar to rate theories, where transitions between the discrete states of the system are exponentially distributed in time and, in particular, one waits an exponentially distributed time in the empty state before an ion enters the channel. The exponential distribution may be considered as arising from the assumption that the ion entry rate into an empty channel does not depend on the time elapsed since the channel last became empty (McGill and Schumaker, 1996). This will often be a good approximation for the entry of distinct ions into the channel, although it

does not capture the fractal character of the trajectories of individual ions.

The electrical distance, f_A^d, appearing in Eqs. 45 and 47 is assigned to the β_R. This means that the entrance rate is independent of Ψ_I. Physically, this choice assumes that entrance is limited by diffusion up to the channel mouth, and not by a local barrier at the channel entrance. Diffusion up to the channel mouth should not be very sensitive to an applied electric field, which would not penetrate far into an electrically conducting solution. In contrast, an applied field might well speed transitions over a local barrier near the membrane surface. The sublinear IV curves observed in the proton conduction experiments of Eisenman et al. (1980), Decker and Levitt (1988), and Akeson and Deamer (1991) at low proton concentrations, where conductance is likely to be limited by entrance, are consistent with the idea that the entrance rate is not strongly dependent on Ψ_I. Even in the absence of a local entrance barrier, however, our assignment of f_A^d neglects interfacial polarization (Andersen, 1983), which becomes significant at low ionic strength and large applied potentials.

The transition probabilities, ν_R, are scaled with n in the same way as γ_i^s and δ_i^s (see Eqs. 23 and 24, note $\Delta\mathcal{L}^s \propto 1/n$). These latter transition probabilities lead to a diffusion process in the limit $n \to \infty$. The scaling of the ν_R is thus consistent with modeling motion of defects from the region of the central barrier to the boundary regions as diffusive. The scaling of the η_R with n is then determined by the constraints given in Eqs. 46 and 48. The assignment of the electrical distances, f_B^d, to the transition probabilities, ν_R, instead of the η_R is arbitrary. But we do not expect these rapid transitions to be rate limiting, so this choice may not be important.

Boundary conditions

In this subsection, we start from expressions for a steady-state flux through the entrances I and II of the pore as described by the random walk in Fig. 2 *C*. Inserting the definitions for the transition probabilities that we have previously obtained, and taking the limit $n \to \infty$, we obtain boundary conditions for the framework model of Fig. 2 *B*. The calculations are straightforward, but somewhat cumbersome. Use of the dimensionless variables described in Appendix A shortens the intermediate expressions.

On side I, balance probability flux in and out of the state H_1 of Fig. 2 *C*. We have

$$Q_1^H(\gamma_1^H + \beta_1) = Q_I^b\alpha_1 C_I + Q_2^H\delta_2^H\,, \tag{56}$$

Substitute in expressions for transition probabilities, Eqs. 23, 24, 49, and 50, as well as the relationship between state probability and density, Eq. 27. Divide by a common factor, rearrange terms, take the limit $n \to \infty$, and, finally, use the definition of J^H, Eq. 31, to obtain (see Appendix A)

$$P^H(-\mu_A^H)\mathcal{L}^H \exp(-\beta f_A^d\Psi_I) = -J^H t^a + Q_I^b a^{-1} e^{\beta\zeta} c_I\,, \tag{57}$$

where $c_I = C_I/C_\bullet$ is the dimensionless concentration.

To complete the analysis of side I, balance flux in and out of state d_n,

$$Q_n^d(\delta_n^d + \nu_I) = Q_I^b\eta_I + Q_{n-1}^d\gamma_{n-1}^d\,. \tag{58}$$

Make the appropriate substitutions, rearrange terms and take the limit $n \to \infty$ to obtain

$$Q_I^b = P^d(\mu_C^d)\mathcal{L}^d a \exp(\beta f_B^d\Psi_I). \tag{59}$$

Similarly, on side II, flux in and out of state H_n is balanced to obtain

$$P^H(\mu_A^H)\mathcal{L}^H \exp(\beta f_A^d\Psi_I) = J^H t^a + Q_{II}^b a^{-1} e^{\beta\zeta} c_{II}\,, \tag{60}$$

and balancing flux in and out of the state d_1 gives

$$Q_{II}^b = P^d(-\mu_C^d)\mathcal{L}^d a\exp(-\beta f_B^d\Psi_I). \tag{61}$$

We can further eliminate Q_I^b and Q_{II}^b from Eqs. 57 and 59–61 to yield

$$P^H(-\mu_A^H)\mathcal{L}^H\exp(-\beta f_A^d\Psi_I) = -J^H t^a + P^d(\mu_C^d)\mathcal{L}^d\exp(\beta(f_B^d\Psi_I + \zeta))c_I\,, \tag{62}$$

$$P^H(\mu_A^H)\mathcal{L}^H\exp(\beta f_A^d\Psi_I) = J^H t^a + P^d(-\mu_C^d)\mathcal{L}^d\exp(\beta(-f_B^d\Psi_I + \zeta))c_{II}\,, \tag{63}$$

Note that these expressions are dimensionless. The density, P^s, has units of inverse reaction coordinate, and the flux, J^s, has units of inverse time.

Expression for a

The dimensionless quantity $\hat{a}$ was originally introduced in Eq. 38 and then expressed in terms of a in Eq. 43. To obtain an expression for a, we set the probability of the boundary states b_I and b_{II} equal to the integral of the Boltzmann factor over the respective boundary regions under the condition of symmetrical equilibrium: $C_I = C_{II}$ and $\Psi_I = 0$. For example

$$Q_I^b = \int_{\mu_C^d}^{\mu_A^d} P^d(\mu^d)\,d\mu^d. \tag{64}$$

At equilibrium, $P^d(\mu^d)$ is given by Eq. 34. Substitute in for Q_I^b using Eq. 59, with $\Psi_I = 0$, and then on both sides for

$P^d(\mu^d)$ using Eq. 34. Solving for a, we obtain

$$a = (\mathcal{L}^d)^{-1} \int_{\mu_C^d}^{\mu_A^d} \exp(-\beta\Delta\Phi^d(\mu^d))\, d\mu^d$$

$$= (\mathcal{L}^d)^{-1} \int_{-\mu_A^d}^{-\mu_C^d} \exp(-\beta\Delta\Phi^d(\mu^d))\, d\mu^d. \quad (65)$$

The value of a is given as an integral over the relative energy, $\Delta\Phi(\mu^d) = \Phi(\mu^d) - \Phi(\mu_C^d)$, and can be evaluated after a choice is made for μ_C^d. Eq. 65 completes the construction of the single proton model using the lumped state approximation. We next show that the model is consistent with statistical mechanics under the condition of symmetrical equilibrium.

EQUILIBRIUM PROBABILITY FOR PROTON OCCUPATION

Insight may be gained into the physical assumptions that lie behind the framework model by comparing the expression for the equilibrium probability of proton occupation of the pore with the analogous expression from statistical mechanics.

Statistical mechanics

For the purpose of constructing a partition function, the total energy of the empty pore includes the energy of a reference proton in solution far away from the channel. Assuming that the reference state is on side I, and approximating activities by concentrations, the energy of the reference proton may be written in the form

$$W_{ref}^H = k_B T \ln C_I/C_H + \Psi_I, \quad (66)$$

where C_H is a constant with units of concentration. According to statistical mechanics, the probability of proton occupation is then equal to

$$Q_{SM}^H = \frac{\int_{-\mu_A^H}^{\mu_A^H} \exp(-\beta W^H(\mu^H))\, d\mu^H}{\int_{-\mu_A^H}^{\mu_A^H} \exp(-\beta W^H(\mu^H))\, d\mu^H + (C_H/C_I)\exp(-\beta\Psi_I)\int_{-\mu_A^H}^{\mu_A^H} \exp(-\beta W^d(\mu^d))\, d\mu^d}. \quad (67)$$

Because the intervals $[-\mu_A^H, \mu_A^H]$ and $[-\mu_A^d, \mu_A^d]$ only include the pore interior, this expression neglects all interactions between the channel and ions in the aqueous solution outside.

Framework model

The equilibrium probability for proton occupation in the framework model is

$$Q_{FW}^H = \int_{-\mu_A^H}^{\mu_A^H} P^H(\mu^H)\, d\mu^H. \quad (68)$$

We also have the normalization condition

$$1 = \int_{-\mu_A^H}^{\mu_A^H} P^H(\mu^H) d\mu^H + \int_{-\mu_C^d}^{\mu_C^d} P^d(\mu^d) d\mu^d + Q_I^b + Q_{II}^b. \quad (69)$$

We construct an expression comparable to that from statistical mechanics by dividing the right-hand side of Eq. 68 by the right-hand side of Eq. 69. Form the ratio and simplify (see Appendix B) to obtain

$$Q_{FW}^H = \frac{\int_{-\mu_A^H}^{\mu_A^H} \exp(-\beta W^H(\mu^H))\, d\mu^H}{\int_{-\mu_A^H}^{\mu_A^H} \exp(-\beta W^H(\mu^H))\, d\mu^H + \frac{\mathcal{L}^H}{\mathcal{L}^d}\frac{C_0}{C_I}\exp(-\beta\Psi_I)\mathcal{A}}, \quad (70)$$

where

$$\mathcal{A} = \int_{-\mu_C^d}^{\mu_C^d} \exp(-\beta W^d(\mu^d))\, d\mu^d + \exp(-\beta\Psi^d(\mu_B^d)) \int_{\mu_C^d}^{\mu_A^d} \exp(-\beta\Phi^d(\mu^d))\, d\mu^d + \exp(-\beta\Psi^d(-\mu_B^d)) \int_{-\mu_A^d}^{-\mu_C^d} \exp(-\beta\Phi^d(\mu^d))\, d\mu^d. \quad (71)$$

To make the correspondence between Q_{FW}^H and Q_{SM}^H, equate the coefficient of the integral in the second term of the denominator of Eq. 67 with the coefficient of $\mathcal{A}$ in Eq. 70. This leads to

$$C_H = (\mathcal{L}^H/\mathcal{L}^d)C_0. \quad (72)$$

With this identification, the equilibrium expressions for Q_{SM}^H and Q_{FW}^H are identical when $\Psi_I = 0$. Under the influence of an applied potential, the framework model makes the approximation

$$\int_{-\mu_A^d}^{\mu_A^d} \exp(-\beta W^d(\mu^d)) d\mu^d \approx \mathcal{A}. \quad (73)$$

The expression for $\mathcal{A}$, Eq. 71, shows that the boundary regions of the framework model act electrically like points.

C_0 is a free parameter in the framework model theory that we have developed thus far, and is combined with the unknown free energy difference, $\Phi_C^d - \Phi_A^H$, between the defect and proton potentials of mean force in the expression for ζ given by Eq. 44. Our analysis of the data of Eisenman et al. (Schumaker et al., 2000) only requires a value for ζ. However, an expression for C_0 can be obtained with the help of the statistical mechanical theory of selective ion channels developed by Roux (1999). This gives C_0 as the inverse of an effective pore volume accessible to the excess proton (Schumaker, manuscript in preparation). This result may be useful for interpreting temperature dependence studies of proton conduction.

GENERAL SOLUTION OF FRAMEWORK MODEL

In Appendix C, we find the general solution for the framework model proton current, J^H. The method of solution depends on solving a linear set of equations, and, in this respect, is similar to that of rate theory. See, for example, Läuger (1973) or Hille and Schwarz (1978).

A linear system of eight equations and eight unknowns is obtained. Two of the equations arise by integrating the Nernst–Planck equations, Eq. 31, for $s \in \{H, d\}$. Four equations come from the boundary conditions, namely Eqs. 57 and 59–61. The seventh equation is the normalization condition, Eq. 69, and the eighth equation is simply the equality of the proton and defect fluxes, $J^H = J^d$, which holds at steady state. The eight corresponding unknowns are the densities at either end of the proton and defect diffusion intervals, namely $P^H(\mu_A^H)$, $P^H(-\mu_A^H)$, $P^d(\mu_C^d)$, and $P^d(-\mu_C^d)$, the probabilities Q_I^b and Q_{II}^b of the defect boundary regions, and the fluxes J^H and J^d. Three variables are quickly eliminated to give a system of five equations in Appendix C, which is then solved.

The solution for the current has the form

$$J^H(c_I, c_{II}, \Psi_I) = \frac{c_I e^{\beta\Psi_I} - c_{II}}{t^H F^H + t^d F^d + t^a F^a}, \tag{74}$$

where the dimensionless variables c_I and c_{II} give the numerical value of the bulk concentrations on either side of the channel in standard units (e.g., moles), and $\beta\Psi_I = eV_I/k_BT$ is proportional to the applied electrical potential, V_I. t^H and t^d are the characteristic times for proton and defect diffusion defined by Eq. 55, and the access time, t^a, is a characteristic time for entrance and exit, processes that were not represented in the molecular dynamics simulations. The coefficients of the characteristic times have the form

$$F^H = F_0^H + F_1^H c_I + F_2^H c_{II}, \tag{75}$$

$$F^d = F_1^d c_I + F_2^d c_{II} + F_3^d c_I c_{II}, \tag{76}$$

$$F^a = F_0^a + F_1^a c_I + F_2^a c_{II}, \tag{77}$$

where the F_i^s are coefficients given in Appendix C.

Note that the coefficient F^d in the denominator of J^H includes a term proportional to the product $c_I c_{II}$. As c_I and c_{II} increase, this term, in principle, gives an eventually decreasing flux, J^H. Single-ion theories that describe the empty channel by a single indivisible state give rise to expressions for J^H whose forms are similar to Eq. 74, but without such quadratic terms in the denominator. This is true for single-ion rate theories (for example, Läuger, 1973) and single-ion diffusion theories (Levitt, 1986; McGill and Schumaker, 1996).

The origin of the quadratic term is reminiscent of the "clogging" mechanism described by Schumaker and MacKinnon (1990). When both c_I and c_{II} are sufficiently high, the system becomes trapped in the proton segment of the state diagram of Fig. 2 *B*. For example, an ion that exits on side II will leave the system in state b_{II}, but an ion entry from side II is likely to occur before the defect reaction coordinate can cross the central barrier to state b_I. This effect reduces the rate of cycling around the diagram and so reduces the flux J^H at very high $c_I c_{II}$.

PROPERTIES OF THE GENERAL SOLUTION

Current symmetry

The gramicidin dimer is symmetrical about its center, $z = 0$, a property reflected in the symmetry of the potentials of mean force calculated by Pomès and Roux (manuscript in preparation): $\Phi^s(\mu^s) = \Phi^s(-\mu^s)$. As a consequence of this and the symmetry properties of the applied potential Ψ about the channel center, the framework model current J, Eq. 74, should have the symmetry

$$J(c_2, c_1, -\Psi) = -J(c_1, c_2, \Psi) \tag{78}$$

for all concentrations c_1 and c_2, as well as electrical potential energies Ψ. Further, the symmetry should hold while the characteristic times, t^s, are varied independently of each other. Write the coefficients F_i^s in the denominator of J, given by Eqs. 75–77, as functions of the applied potential: $F_i^s = F^s{}_i(\Psi_I)$. Then the current symmetry holds if and only if the coefficients have the properties,

$$F_0^s(-\Psi) = e^{-\beta\Psi} F_0^s(\Psi), \tag{79}$$

$$F_2^s(-\Psi) = e^{-\beta\Psi} F_1^s(\Psi), \tag{80}$$

$$F_3^s(-\Psi) = e^{-\beta\Psi} F_3^s(\Psi), \tag{81}$$

In Appendix D, we demonstrate that these coefficient symmetries hold.

Saturating current at high voltage

At very high applied potentials, it is reasonable to expect that the proton current through gramicidin should saturate at a finite value. This is because one would not expect the applied potential to reach far into the aqueous solutions on either side of the membrane, because these solutions are electrical conductors. This reasoning is consistent with IV measurements through gramicidin by Akeson and Deamer (1991). However, it ignores the effects of interfacial polarization, which were measured by Andersen (1983) for the conduction of several different cations through gramicidin at low ionic strength.

The framework model is constructed to give the saturating behavior; the entrance rate constants, $\alpha_R C_R$, are independent of the applied potential Ψ_I, see Eq. 49. In Appendix E, the limiting current is calculated to be

$$\lim_{\Psi_I \to \infty} J = c_I (t^a a)^{-1} e^{\beta\zeta}. \tag{82}$$

This result is easily understood in view of the expression for $\alpha_R C_R$ given by Eq. 49. The saturating current is simply the entrance rate: the transition probability divided by the time step Δt.

Equilibrium conductance

The conductance at Nernst equilibrium is defined by

$$G_{Eq} = \left.\frac{dI}{dV_I}\right|_{Eq} = e_0^2 \frac{dJ^H}{d\Psi_I}, \tag{83}$$

where $I = e_0 J^H$ is the current through the channel. Appendix F shows how this quantity is computed from Eq. 74 and that the denominator can be written in a surprisingly compact form. The result simplifies even further under the condition of a symmetrical equilibrium, with $c_I = c_{II} = c$ and $\Psi_I = 0$. Denoting by G_0 the conductance evaluated at symmetrical equilibrium, we find

$$G_0 = \frac{e_0^2}{k_B T} \frac{c}{[(t^H h_0^H + 2t^a) e^{-\beta\zeta} + t^d h_0^d c](g_1^d + g_0^H e^{\beta\zeta} c)}, \tag{84}$$

where

$$h_0^H = (\mathscr{L}^H)^{-1} \int_{-\mu_A^H}^{\mu_A^H} \exp(\beta \Delta\Phi^H(\mu)) d\mu, \tag{85}$$

$$h_0^d = (\mathscr{L}^d)^{-1} \int_{-\mu_C^d}^{\mu_C^d} \exp(\beta \Delta\Phi^d(\mu)) d\mu, \tag{86}$$

$$g_0^H = (\mathscr{L}^H)^{-1} \int_{-\mu_A^H}^{\mu_A^H} \exp(-\beta \Delta\Phi^H(\mu)) d\mu, \tag{87}$$

$$g_1^d = (\mathscr{L}^d)^{-1} \int_{-\mu_A^d}^{\mu_A^d} \exp(-\beta \Delta\Phi^d(\mu)) d\mu. \tag{88}$$

The first two terms in the expression for ζ, Eq. 44, give the free energy difference between the proton and defect potentials of mean force. The denominator of Eq. 84 contains terms proportional to both $e^{\beta\zeta}$ and $e^{-\beta\zeta}$. Consequently, the conductance decreases if the free energy difference between the profiles is either sufficiently large and positive or sufficiently large and negative.

The conductance also decreases if the $\Delta\Phi^s$ have shapes with high maxima (the h_0^s are large) or deep minima (the g_0^s are large). Conductance is maximum when the $\Delta\Phi^s$ are relatively flat and the magnitude of the energy difference, ζ, is not too large. Finally, notice that the denominator of G_0 is quadratic in c, reflecting the quadratic dependence of the denominator of J, Eq. 74, on concentration.

NUMERICAL SOLUTION

Numerical simulations of random walks are used by Schumaker et al. (2000) to qualitatively demonstrate the nature of the trajectories underlying the single proton conduction model. They may also represent an interesting alternative method for generating Brownian dynamics simulations (for example, Jakobsson and Chiu, 1987). In this section, we describe how to construct simulations corresponding to the analytical theory.

The random walk shown in Fig. 2 *C* is convenient for construction of the framework model, but less suitable for numerical simulation. Instead, the numerical simulation takes place on the symmetrized random walk shown in Fig. 2 *D*. To account for the additional state, we replace $n \to n + 1$ in the formula for the time step, Eq. 20, and in the formulas for the entrance and exit transition probabilities, Eqs. 49–54. These formulas then define the simulated random walk.

According to Eq. 27, each random walk gridpoint corresponds to a reaction coordinate subinterval of width $\Delta\mathscr{L}^s$. This is true even for the symmetrized endpoints $i = 0$ and $i = n$ corresponding to coordinates $\mu^d = \pm\mu_C^d$. The symmetrized random walk should then most appropriately be identified with diffusion on the interval $\pm(1 + 1/n)\mu_C^d$. For this reason, we compare analytical results using the value for a given by Eq. 65 with numerical results using the modified value

$$a_{sim} = (\mathscr{L}^d)^{-1} \int_{(1+1/n)\mu_C^d}^{\mu_A^d} \exp(-\beta \Delta\Phi^d(\mu^d)) d\mu^d. \tag{89}$$

In the simulations, half of the probabilities associated with the endpoints $i = 0$ and $i = n$ are added to the boundary state probabilities Q_I^b and Q_{II}^b, respectively. With our defi-

nition of the symmetrized random walk, use of a_{sim} and this treatment of probability is necessary for the good agreement between the simulated and exact probability densities described below. However, this method of simulating the boundary conditions has an ad hoc character and can undoubtedly be improved.

The simulated random walk is discrete in both time and space, conforming to the theoretical discussion. Because of the large difference between the proton and defect diffusion coefficients obtained from molecular dynamics (Schumaker et al., 2000), transition rates on the proton segment of the state diagram are much higher than those on the defect segment. To retain numerical efficiency, different values of $\Delta\tau$ are used to describe proton and defect diffusion. For the same reason, dwell times in the states b_I and b_{II} are calculated from geometric distributions directly, without taking time steps, similar to the method used to calculate exit from the empty state of the single ion model (McGill and Schumaker, 1996).

Proton and defect probability densities are shown in Fig. 3, *A* and *B*. These runs use the potentials of mean force and diffusion coefficients obtained from the molecular dynamics simulations of Pomès and Roux (manuscript in preparation), and shown in Fig. 1, *B* and *C*. Densities shown in Fig. 3 represent the average of four simulations of about 2.1×10^9 time steps each. Each of the four simulations was given a different seed to initialize the random number generator (*ran*2, described by Press et al., 1992) but all other parameter values were kept the same. In making these calculations, the intrinsic potentials are interpolated linearly between grid points where potentials of mean force were calculated by molecular dynamics. The piecewise smooth character of the probability densities is due to the piece-wise linearity of the interpolated potentials.

The simulated and exact proton densities are very similar in both shape and amplitude. The integrated probability of the simulated proton density is only about 0.5% greater than that of the exact solution for the proton density. This excellent agreement is in part fortuitous, because only 896 protons entered and left the pore in the simulations that produced Fig. 3. If we estimate the uncertainty in this number as $896^{1/2}$, the corresponding variation in the probability for proton occupation is about 3.3%. In a second simulation, made using a different parameter set, the difference between the simulated and exact proton occupation probability was slightly larger than the estimate based on the square root of the number of protons that enter the pore (results not shown). For the simulation used to make Fig. 3, the defect density and boundary state probabilities Q_I^b and Q_{II}^b are also in excellent agreement with the exact solution.

Fig. 4 shows the current through the framework model as a function of applied voltage. The exact solution of the framework model is compared with simulations at 50, 100, and 200 mV applied potential. Agreement is very good. We have also used the numerical simulation method to calculate mean first passage times across the defect potential barrier as a function of applied potential, following the protocol used to construct Fig. 5 in Schumaker et al. (2000). Mean first passage times obtained by the simulation method are in excellent agreement with those results (unpublished).

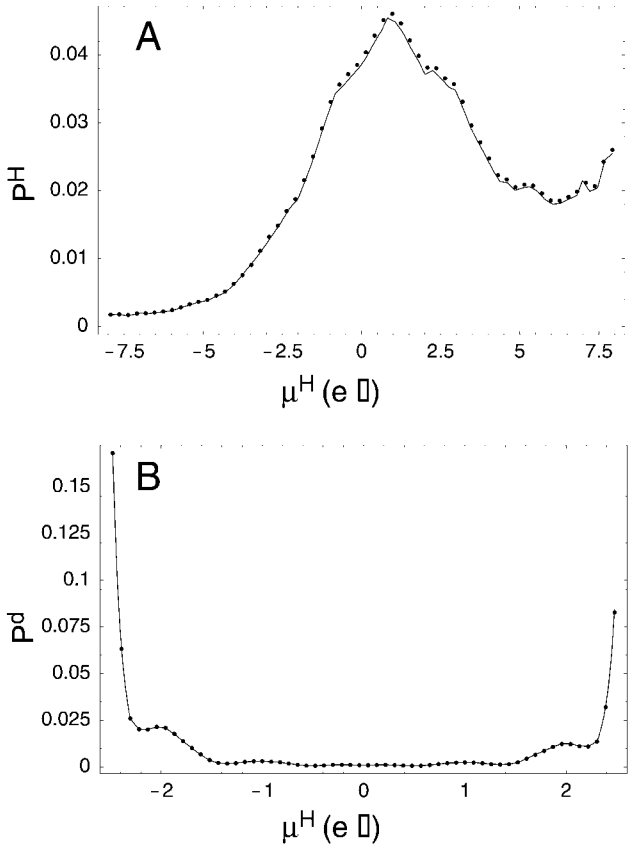

FIGURE 3 Exact and simulated framework model probability densities. The analytical solution of the framework model is given by the solid curves, and results of numerical simulations are given by the dots. Proton and defect trajectories were simulated on the symmetrized random walk shown in Fig. 2 *D* with $n = 57$. Densities were obtained by averaging together the results of four runs of about 2.1×10^9 time steps each. $C_I = C_{II} = 0.01$ M and $V_I = 100$ mV. Parameter values are $\chi_A^H = 3.35$, $\chi_A^d = 8.1$, $\chi_B^d = 6.8$, and $\chi_C^d = 5.7$ with $\alpha = 0.4348$ and scaling $\mu^d = \alpha\chi^d$ (see Schumaker et al., 2000). In addition, $\zeta = 3.60$ and $t^a = 23.5$ ns. (*A*) Density on the proton segment for $-\mu_A^H < \mu^H < \mu_A^H$. (*B*) Density on the defect segment for $-\mu_C^d < \mu^d < \mu_C^d$. The analytical solutions for the probabilities of the boundary regions on either side of the defect interval are $Q_I^b = 0.440$ and $Q_{II}^b = 0.188$. Numerically estimated values of these probabilities are $Q_I^b = 0.438$ and $Q_{II}^b = 0.184$.

DISCUSSION

We have constructed a framework model for single proton conductance through gramicidin, a model designed to incorporate the results of molecular dynamics simulations (Pomès and Roux, 1996, 1997, and manuscript in preparation) and used it to predict conductance properties. Such models are currently necessary to bridge the gap in time

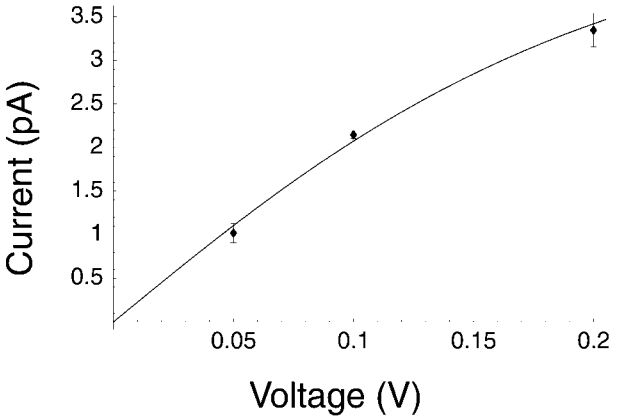

FIGURE 4 Exact and simulated framework model proton current. The figure shows current I as a function of applied voltage under the same conditions as in Fig. 3. The analytical solution of the framework model, Eq. 74, is shown by the solid curve. Error bars show twice the standard deviation of the mean for the four runs described in the legend of Fig. 3.

scales between molecular dynamics simulations and electrophysiology. The framework model consists of a coupled pair of Nernst–Planck equations describing the diffusion of the axial component of the pore dipole moment in the presence or in the absence of an excess proton in the chain of water molecules occupying the gramicidin pore. In the absence of an excess proton, the dipole moment parameterizes the reorientation of the pore waters from a configuration in which the axial component of their dipole moments point in the $-z$ direction to a configuration in which the axial component points in the $+z$ direction. The simulations suggest that water reorientation is mediated by a defect in the hydrogen bond structure that passes through the water chain. Therefore, we also describe the empty or neutral channel as one in which a defect occupies the pore.

The Nernst–Planck equations and their boundary conditions are obtained as the limit of a sequence of random walks. By the random walk construction, the boundary conditions restrict the model to describing a single diffusing proton or a single diffusing defect. In other words, we construct a diffusion process on a simplified configuration space for proton conduction through gramicidin, portrayed by the state diagram shown in Fig. 2 *B*. This is much different from Goldman–Hodgkin–Katz theory (Hille, 1992) or Poisson Nernst–Planck theories (for example, Chen, 1997), which are mean field theories. In these latter cases, a solution corresponds to a superposition of many different occupancy states of ions in the pore.

From the simulations, we obtain the potential of mean force for proton and defect diffusion through the pore as well as estimates of the proton and defect diffusion coefficients (Schumaker et al., 2000). The proton potential of mean force, shown in Fig. 1 *B,* has the form of a shallow potential well. Transport across such a profile is not described well by rate theories, which are based on asymptotic approximations to diffusion over energy barriers (Cooper et al., 1985, 1988). The defect potential of mean force has the form of a high central barrier separating potential minima. The potentials and diffusion coefficients, obtained from molecular dynamics, completely determine the description of transport in the pore interior. By incorporating this information from the simulation, the framework model can describe this portion of the permeation process without adjustable parameters.

However, the simulations of Pomès and Roux do not address the processes of ion entrance and exit. Here, it is necessary for the framework model to introduce some description. We take a very simple and phenomenological approach. Proton entrances on a given side are assumed to be exponentially distributed in time when the channel is accessible to occupation. The entrance process is then described by a single adjustable parameter, the mean time before a proton enters an empty channel. This is the same description of ion entrance as is implicit in rate theories. The exit process must then satisfy detailed balance with entrance at equilibrium. It also involves a single adjustable parameter, which would be known if the absolute free energy difference between the proton and defect potentials of mean force were known. Finally, there is a third adjustable parameter, which is also concerned with the ion entrance and exit process. This is due to the fact that the state of the waters in the empty channel is not precisely known just as an excess proton leaves or enters; instead, the dipole moment of the empty channel may be in one of the boundary regions of Fig. 1 *C*. The width of these regions is the third parameter. In practice, a reasonable value for this parameter can be chosen, encompassing the potential minima on either side of the central barrier (Schumaker, et al. 2000). Only the two parameters controlling the entrance and exit rates need be optimized to make a comparison with experiment.

The conduction mechanism of our framework model is easily grasped by means of a state diagram, which is analogous to those that describe rate theory permeation models, see Fig. 2 *B*. As a proton passes through the channel, say from side I to side II, the proton reaction coordinate follows its progress on the upper segment of the diagram from left to right. The proton exits the channel, leaving water molecules partially aligned. This corresponds to the lumped state b_{II}. The dipole moment of the water chain must then turn to become receptive to another proton entering on side I. The molecular dynamics simulations (Pomès and Roux, 1997, and manuscript in preparation) suggest that turning is mediated by a defect in the hydrogen bond structure that passes through the water chain. This defect is followed by the reaction coordinate that parameterizes the lower segment of the state diagram, from right to left. When the reaction coordinate is in the lumped state b_{I}, the system is ready to accept another free proton from side I.

The most problematic feature of this model may be the treatment of the boundary conditions. An important com-

ponent of the configuration space is missing, which was pointed out following the statistical mechanical expression for the probability of proton occupation, Eq. 67. Therefore, there is no description of the interaction of the channel with excess protons outside, but close to, the entrance. For example, it is plausible that water dipoles are partially oriented by nearby protons before they enter the channel. In contrast, our model implicitly assumes that the orientation of channel waters is independent of excess protons on the outside, and that proton entrance only becomes possible when the water dipoles happen to be favorably aligned. To test this assumption and possibly construct a more realistic model, it would be very useful to have molecular dynamics simulations of the ion entrance process.

APPENDIX A: DIMENSIONLESS VARIABLES AND BOUNDARY CONDITIONS

Results in the body of this paper are given in dimensional form, but many calculations become less cumbersome when dimensionless variables are used. Reaction coordinate intervals over which proton or defect diffusion is described are conveniently rescaled to [0, 1]. Let

$$\xi^{\mathrm{H}} = (1 + \mu^{\mathrm{H}}/\mu_{\mathrm{A}}^{\mathrm{H}})/2, \tag{90}$$

$$\xi^{\mathrm{d}} = (1 + \mu^{\mathrm{d}}/\mu_{\mathrm{C}}^{\mathrm{d}})/2. \tag{91}$$

Then the random walk of Fig. 2 *C* takes place on the grid points $\xi_{\mathrm{i}}^{\mathrm{s}} = i/n$, $\{i = 1, 2, \ldots, n\}$.

Dimensionless energies are defined: $\phi^{\mathrm{s}}(\xi^{\mathrm{s}}) = \beta\Phi^{\mathrm{s}}(\mu^{\mathrm{s}})$, $\Delta\phi^{\mathrm{s}}(\xi^{\mathrm{s}}) = \beta\Delta\Phi^{\mathrm{s}}(\mu^{\mathrm{s}})$, $\psi^{\mathrm{s}}(\xi^{\mathrm{s}}) = \beta\Phi^{\mathrm{s}}(\mu^{\mathrm{s}})$, and $w^{\mathrm{s}}(\xi^{\mathrm{s}}) = \beta W^{\mathrm{s}}(\mu^{\mathrm{s}})$. For the energy due to the applied potential, write $\psi_{\mathrm{I}} = \beta\Psi_{\mathrm{I}}$. The dimensionless probability density is $p^{\mathrm{s}}(\xi^{\mathrm{s}}) = P^{\mathrm{s}}(\mu^{\mathrm{s}})\mathscr{L}^{\mathrm{s}}$. Electrical potential energies, corresponding to Eqs. 5 and 6, can then be written:

$$\psi^{\mathrm{H}}(\xi^{\mathrm{H}}) = \psi_{\mathrm{I}}/2 - f^{\mathrm{H}}(2\xi^{\mathrm{H}} - 1)\psi_{\mathrm{I}}/2, \tag{92}$$

$$\psi^{\mathrm{d}}(\xi^{\mathrm{d}}) = -f_{\mathrm{C}}^{\mathrm{d}}(2\xi^{\mathrm{d}} - 1)\psi_{\mathrm{I}}/2. \tag{93}$$

For the derivation of the boundary conditions, it is helpful to use the compact notation, $w_{\mathrm{i}}^{\mathrm{s}} = w^{\mathrm{s}}(\xi_{\mathrm{i}}^{\mathrm{s}})$ and $w_{\mathrm{i}}^{\mathrm{s}\prime} = w^{\mathrm{s}\prime}(\xi_{\mathrm{i}}^{\mathrm{s}})$, where the prime denotes a derivative with respect to the argument. The transition probabilities can then be written as

$$\gamma_{\mathrm{i}}^{\mathrm{s}} = \Delta t(t^{\mathrm{s}})^{-1}n^2\left\{1 - \frac{w_{\mathrm{i}}^{\mathrm{s}\prime}}{(2n)} + \frac{\hat{\epsilon}_{\mathrm{i}}^{\mathrm{s}}}{n^2} + \mathbb{O}(n^{-3})\right\}, \tag{94}$$

$$\delta_{\mathrm{i}}^{\mathrm{s}} = \Delta t(t^{\mathrm{s}})^{-1}n^2\left\{1 + \frac{w_{\mathrm{i}}^{\mathrm{s}\prime}}{(2n)} + \frac{\hat{\epsilon}_{\mathrm{i}}^{\mathrm{s}}}{n^2} + \mathbb{O}(n^{-3})\right\}, \tag{95}$$

where t^{s} is given by Eq. 55 and

$$\hat{\epsilon}_{\mathrm{i}}^{\mathrm{s}} = -w^{\mathrm{s}\prime\prime}(\xi_{\mathrm{i}}^{\mathrm{s}})/4 + w^{\mathrm{s}\prime}(\xi_{\mathrm{i}}^{\mathrm{s}})^2/8. \tag{96}$$

Insert Eqs. 94, 95, 49, and 50 into Eq. 56 and let $n \to \infty$ to obtain

$$0 = (t^{\mathrm{H}})^{-1}[p^{\mathrm{H}\prime}(0) + w^{\mathrm{H}\prime}(0)p^{\mathrm{H}}(0)] - (t^{\mathrm{a}})^{-1}p^{\mathrm{H}}(0)e^{-f_{\mathrm{A}}^{\mathrm{d}}\psi_{\mathrm{I}}} + (t^{\mathrm{a}})^{-1}Q_{\mathrm{I}}^{\mathrm{b}}a^{-1}e^{\beta\zeta}c_{\mathrm{I}}. \tag{97}$$

This equation can be simplified by noting that the Nernst–Planck equation, Eq. 31, can be written in terms of dimensionless variables as

$$J^{\mathrm{s}} = -(t^{\mathrm{s}})^{-1}[p^{\mathrm{s}\prime}(\xi^{\mathrm{s}}) + w^{\mathrm{s}\prime}(\xi^{\mathrm{s}})p^{\mathrm{s}}(\xi^{\mathrm{s}})]. \tag{98}$$

Substitution of this expression into Eq. 97 gives Eq. 57.

APPENDIX B: EQUILIBRIUM PROBABILITY FOR PROTON OCCUPATION

This appendix shows how Eq. 70 is obtained from Eqs. 68 and 69. To begin, consider the Boltzmann distribution of the density P^{H} at equilibrium, Eq. 34 with $s = H$. From this equation, obtain an expression for $P^{\mathrm{H}}(\mu^{\mathrm{H}})$ in terms of $P^{\mathrm{H}}(-\mu_{\mathrm{A}}^{\mathrm{H}})$ by eliminating K^{H}. Integrate the result to find

$$\int_{-\mu_{\mathrm{A}}^{\mathrm{H}}}^{\mu_{\mathrm{A}}^{\mathrm{H}}} P^{\mathrm{H}}(\mu^{\mathrm{H}})\,\mathrm{d}\mu^{\mathrm{H}} = P^{\mathrm{H}}(-\mu_{\mathrm{A}}^{\mathrm{H}})\exp(\beta W^{\mathrm{H}}(-\mu_{\mathrm{A}}^{\mathrm{H}}))\int_{-\mu_{\mathrm{A}}^{\mathrm{H}}}^{\mu_{\mathrm{A}}^{\mathrm{H}}} \exp(-\beta W^{\mathrm{H}}(\mu^{\mathrm{H}}))\,\mathrm{d}\mu^{\mathrm{H}}. \tag{99}$$

Next, consider the second integral in Eq. 69. Use the Boltzmann distribution at equilibrium to solve for $P^{\mathrm{d}}(\mu^{\mathrm{d}})$ in terms of $P^{\mathrm{d}}(\mu_{\mathrm{C}}^{\mathrm{d}})$ and integrate to obtain

$$\int_{-\mu_{\mathrm{C}}^{\mathrm{d}}}^{\mu_{\mathrm{C}}^{\mathrm{d}}} P^{\mathrm{d}}(\mu^{\mathrm{d}})\,\mathrm{d}\mu^{\mathrm{d}} = P^{\mathrm{d}}(\mu_{\mathrm{C}}^{\mathrm{d}})\exp(\beta W^{\mathrm{d}}(\mu_{\mathrm{C}}^{\mathrm{d}}))\int_{-\mu_{\mathrm{C}}^{\mathrm{d}}}^{\mu_{\mathrm{C}}^{\mathrm{d}}} \exp(-\beta W^{\mathrm{d}}(\mu^{\mathrm{d}}))\,\mathrm{d}\mu^{\mathrm{d}}. \tag{100}$$

We now consider $Q_{\mathrm{I}}^{\mathrm{b}}$. Start with Eq. 59 and substitute the middle expression for *a* from Eq. 65. Transform the exponent using, from Eqs. 6 and 14,

$$f_{\mathrm{B}}^{\mathrm{d}}\Psi_{\mathrm{I}} = \Psi^{\mathrm{d}}(\mu_{\mathrm{C}}^{\mathrm{d}}) - \Psi^{\mathrm{d}}(\mu_{\mathrm{B}}^{\mathrm{d}}), \tag{101}$$

to obtain

$$Q_{\mathrm{I}}^{\mathrm{b}} = P^{\mathrm{d}}(\mu_{\mathrm{C}}^{\mathrm{d}})\exp(W^{\mathrm{d}}(\mu_{\mathrm{C}}^{\mathrm{d}})\}\exp(-\beta\Psi^{\mathrm{d}}(\mu_{\mathrm{B}}^{\mathrm{d}}))\int_{\mu_{\mathrm{C}}^{\mathrm{d}}}^{\mu_{\mathrm{A}}^{\mathrm{d}}} \exp(-\beta\Phi^{\mathrm{d}}(\mu^{\mathrm{d}}))\,\mathrm{d}\mu^{\mathrm{d}}. \tag{102}$$

Finally, consider the probability $Q_{\mathrm{II}}^{\mathrm{b}}$ appearing in Eq. 69. Obtain a new expression by considering Eq. 61. The term $P^{\mathrm{d}}(-\mu_{\mathrm{C}}^{\mathrm{d}})$ can be written in terms of $P^{\mathrm{d}}(\mu_{\mathrm{C}}^{\mathrm{d}})$ by using the Boltzmann distribution for P^{d}, Eq. 34, and eliminating K^{d}. Substitute the last expression for *a* from Eq. 65. The exponent can be simplified using

$$f_{\mathrm{B}}^{\mathrm{d}}\Psi_{\mathrm{I}} = -\Psi^{\mathrm{d}}(-\mu_{\mathrm{C}}^{\mathrm{d}}) + \Psi^{\mathrm{d}}(-\mu_{\mathrm{B}}^{\mathrm{d}}) \tag{103}$$

yielding

$$Q_{\mathrm{II}}^{\mathrm{b}} = P^{\mathrm{d}}(\mu_{\mathrm{C}}^{\mathrm{d}})\exp(W^{\mathrm{d}}(\mu_{\mathrm{C}}^{\mathrm{d}}))\exp(-\beta\Psi^{\mathrm{d}}(-\mu_{\mathrm{B}}^{\mathrm{d}}))\times\int_{-\mu_{\mathrm{A}}^{\mathrm{d}}}^{-\mu_{\mathrm{C}}^{\mathrm{d}}} \exp(-\beta\Phi^{\mathrm{d}}(\mu^{\mathrm{d}}))\,\mathrm{d}\mu^{\mathrm{d}}. \tag{104}$$

We now divide the right-hand side of Eq. 68 by the right-hand side of Eq. 69 and substitute the results of Eqs. 99, 100, 102, and 104 to obtain

$$Q^{\mathrm{H}}_{\mathrm{FW}} = \frac{\int_{-\mu^{\mathrm{H}}_{\mathrm{A}}}^{\mu^{\mathrm{H}}_{\mathrm{A}}} \exp(-\beta \mathcal{W}^{\mathrm{H}}(\mu))\mathrm{d}\mu}{\int_{-\mu^{\mathrm{H}}_{\mathrm{A}}}^{\mu^{\mathrm{H}}_{\mathrm{A}}} \exp(-\beta \mathcal{W}^{\mathrm{H}}(\mu))\mathrm{d}\mu + \mathcal{A}\mathcal{B}}, \tag{105}$$

where $\mathcal{A}$ is given by Eq. 71 and

$$\mathcal{B} = P^{\mathrm{d}}(\mu^{\mathrm{d}}_{\mathrm{C}})P^{\mathrm{H}}(-\mu^{\mathrm{H}}_{\mathrm{A}})^{-1}\exp(\beta[\mathcal{W}^{\mathrm{d}}(\mu^{\mathrm{d}}_{\mathrm{C}}) - \mathcal{W}^{\mathrm{H}}(-\mu^{\mathrm{H}}_{\mathrm{A}})]). \tag{106}$$

$\mathcal{B}$ can be transformed by substituting from Eq. 62 evaluated at equilibrium. Further, use the definitions associated with the potentials Φ^s and Ψ^s to find

$$\mathcal{W}^{\mathrm{d}}(\mu^{\mathrm{d}}_{\mathrm{C}}) - \mathcal{W}^{\mathrm{H}}(-\mu^{\mathrm{H}}_{\mathrm{A}}) = \Phi^{\mathrm{d}}_{\mathrm{C}} - \Phi^{\mathrm{H}}_{\mathrm{A}} - \frac{\Psi_{\mathrm{I}}}{2} - \frac{(f^{\mathrm{H}} + f^{\mathrm{d}}_{\mathrm{C}})\Psi_{\mathrm{I}}}{2}, \tag{107}$$

leading to

$$\mathcal{B} = (\mathcal{L}^{\mathrm{H}}/\mathcal{L}^{\mathrm{d}})(C_{\mathrm{I}}/C_{\mathrm{I}})\exp(\beta[\Phi^{\mathrm{d}}_{\mathrm{C}} - \Phi^{\mathrm{H}}_{\mathrm{A}} - \Psi_{\mathrm{I}} - \zeta]). \tag{108}$$

Simplifying the exponent using Eq. 44 finally yields Eq. 70.

APPENDIX C: GENERAL SOLUTION OF THE FRAMEWORK MODEL

In this section, we find the general solution for the framework model proton current. We will obtain a system of eight equations for eight unknowns. Calculations are somewhat less cumbersome when made in terms of the dimensionless variables defined in Appendix A. Further, many equations can be written in parallel for the proton and defect species. We will use the superscript s to denote either protons, $s = H$, or defects, $s = d$. In this notation, the eight unknowns are the densities at either end of the proton and defect diffusion intervals, namely $p^s(0)$ and $p^s(1)$, the probabilities $Q^{\mathrm{b}}_{\mathrm{I}}$ and $Q^{\mathrm{b}}_{\mathrm{II}}$ of the defect boundary regions, and the proton and defect fluxes, J^s.

The first equation is simply $J^{\mathrm{H}} = J^{\mathrm{d}}$, which must hold at steady state. This is immediately eliminated by introducing a common variable for the flux, $J = J^s$. The boundary conditions, Eqs. 59 and 61–63, give us four more equations. Written in terms of dimensionless variables, these are

$$Q^{\mathrm{b}}_{\mathrm{I}} = p^{\mathrm{d}}(1)a\,\exp(f^{\mathrm{d}}_{\mathrm{B}}\psi_{\mathrm{I}}), \tag{109}$$

$$Q^{\mathrm{b}}_{\mathrm{II}} = p^{\mathrm{d}}(0)a\,\exp(-f^{\mathrm{d}}_{\mathrm{B}}\psi_{\mathrm{I}}), \tag{110}$$

$$p^{\mathrm{H}}(0)\exp(-f^{\mathrm{d}}_{\mathrm{A}}\psi_{\mathrm{I}}) = -Jt^{\mathrm{a}} + p^{\mathrm{d}}(1)\exp(f^{\mathrm{d}}_{\mathrm{B}}\psi_{\mathrm{I}} + \beta\zeta)c_{\mathrm{I}}, \tag{111}$$

$$p^{\mathrm{H}}(1)\exp(f^{\mathrm{d}}_{\mathrm{A}}\psi_{\mathrm{I}}) = Jt^{\mathrm{a}} + p^{\mathrm{d}}(0)\exp(-f^{\mathrm{d}}_{\mathrm{B}}\psi_{\mathrm{I}} + \beta\zeta)c_{\mathrm{II}}, \tag{112}$$

The sixth and seventh equations are obtained by integrating the Nernst–Planck equation, Eq. 31, which, in terms of dimensionless variables, is Eq. 98. Multiply by an integrating factor and integrate to get

$$-\mathcal{J}^s t^s \int_0^{\xi^s} \exp(w^s(\eta))\,\mathrm{d}\eta = p^s(\xi^s)\exp(w^s(\xi^s)) - p^s(0)\exp(w^s(0)). \tag{113}$$

Note that $w^s(\xi) = \phi^s(\xi) + \psi^s(\xi)$, where the $\psi^s(\xi)$ are given by Eqs. 92 and 93. It is convenient to define the integrals

$$h^s(\xi) = \int_0^{\xi} \exp(\Delta\phi^s(\eta) - f^s(2\eta - 1)\psi_{\mathrm{I}}/2)\,\mathrm{d}\eta, \tag{114}$$

where we use $f^{\mathrm{d}} = f^{\mathrm{d}}_{\mathrm{C}}$ and denote $h^s = h^s(1)$. Then evaluate Eq. 113 at $\xi^s = 1$ and divide by a common factor to get

$$-\mathcal{J}^s t^s h^s = p^s(1)\exp(-f^s\psi_{\mathrm{I}}/2) - p^s(0)\exp(f^s\psi_{\mathrm{I}}/2). \tag{115}$$

This is the form of the integrated Nernst–Planck equation to be used for the general solution.

The eighth equation is obtained from the normalization condition, which we write in terms of dimensionless variables

$$\int_0^1 p^{\mathrm{H}}(\xi)\mathrm{d}\xi + \int_0^1 p^{\mathrm{d}}(\xi)\mathrm{d}\xi + Q^{\mathrm{b}}_{\mathrm{I}} + Q^{\mathrm{b}}_{\mathrm{II}} = 1. \tag{116}$$

We proceed to express the integrals in terms of J and $p^s(0)$. Solve Eq. 113 for $p^s(\xi^s)$ and integrate to get

$$\int_0^1 p^s(\xi)\mathrm{d}\xi = -\mathcal{J}^s t^s \int_0^1 \exp(-w^s(\xi)) \int_0^{\xi} \exp(w^s(\eta))\mathrm{d}\eta\mathrm{d}\xi + p^s(0)\exp(w^s(0)) \int_0^1 \exp(-w^s(\xi))\mathrm{d}\xi. \tag{117}$$

The following difference of energies will be useful,

$$w^s(\eta) - w^s(\xi) = \Delta\phi^s(\eta) - \frac{f^s(2\eta - 1)\psi_{\mathrm{I}}}{2} - \Delta\phi^s(\xi) + \frac{f^s(2\xi - 1)\psi_{\mathrm{I}}}{2}. \tag{118}$$

Then, the second term on the right-hand side of Eq. 117 can be rewritten using

$$\exp(w^s(0)) \int_0^1 \exp(-w^s(\xi))\,\mathrm{d}\xi = \exp(f^s\psi_{\mathrm{I}}/2)g^s, \tag{119}$$

where we define the integral

$$g^s = \int_0^1 \exp(-\Delta\phi^s(\xi) + f^s(2\xi - 1)\psi_{\mathrm{I}}/2)\mathrm{d}\xi. \tag{120}$$

Further, define

$$i^s = \int_0^1 \exp(-w^s(\xi)) \int_0^{\xi} \exp(w^s(\eta))\mathrm{d}\eta\mathrm{d}\xi = \int_0^1 \exp(-\Delta\phi^s(\xi) + f^s(2\xi - 1)\psi_{\mathrm{I}}/2)h^s(\xi)\mathrm{d}\xi, \tag{121}$$

where Eq. 118 and the definition, Eq. 114, are used to obtain the second expression. Use this result and Eq. 119 to rewrite Eq. 117 as

$$\int_0^1 p^s(\xi)d\xi = -Jt^s i^s + p^s(0)\exp(f^s\psi_l/2)g^s. \quad (122)$$

Substituting this expression and the boundary conditions, Eqs. 109 and 110, into the normalization condition, Eq. 116, we have the final form for the eighth equation,

$$-Jt^H i^H + p^H(0)\exp(f^H\psi_l/2)g^H - Jt^d i^d + p^d(0)\exp(f_C^d\psi_l/2)g^d + p^d(1)a\exp(f_B^d\psi_l) + p^d(0)a\exp(-f_B^d\psi_l) = 1. \quad (123)$$

We now have a system of five equations and five unknowns. The equations include the boundary conditions, Eqs. 111 and 112, the integrated Nernst–Planck Eqs. 115, and the normalization condition, Eq. 123. The unknowns are the proton and defect densities at the ends of their intervals, $p^s(0)$ and $p^s(1)$, and the common current J.

These equations may be solved by straightforward algebra. For example, eliminate $p^H(0)$ and $p^H(1)$ by substituting from Eqs. 111 and 112 into Eq. 115 (for $s = H$) and Eq. 123. Then solve for $p^d(0)$ in Eq. 115 (for $s = d$) and use this to eliminate $p^d(0)$ in the two remaining equations. This leaves a system of two equations for the unknowns $p^d(1)$ and J. These can be finally solved for J to obtain Eq. 74. In these calculations, there are several points where Eq. 16 may be used to simplify an exponent.

In the denominator of J, the coefficient F^H is given by Eq. 75, where

$$F_0^H = h^H[g^d + 2a\cosh(f_B^d + f_C^d/2)\psi_l]e^{\psi_h/2-\beta\zeta}, \quad (124)$$

$$F_1^H = (-i^H + h^H g^H)e^{\psi_l}, \quad (125)$$

$$F_2^H = i^H. \quad (126)$$

The coefficient F^d is given by Eq. 76, where

$$F_1^d = [-i^d + h^d g^d + h^d a\exp(f_B^d + f_C^d/2)\psi_l)]\exp(\psi_l, \quad (127)$$

$$F_2^d = i^d + h^d a\exp(f_B^d + f_C^d/2)\psi_l, \quad (128)$$

$$F_3^d = g^H h^d \exp(\psi_l/2 + \beta\zeta). \quad (129)$$

Finally, the coefficient F^a is given by Eq. 77, where

$$F_0^a = 2\exp(\psi_l/2 - \beta\zeta)[g^d + 2a\cosh(f_B^d + f_C^d/2)\psi_l] \times \cosh(f_A^d + f^H/2)\psi_l, \quad (130)$$

$$F_1^a = g^H\exp(1 - f_A^d - f^H/2)\psi_l, \quad (131)$$

$$F_2^a = g^H\exp((f_A^d + f^H/2)\psi_l). \quad (132)$$

APPENDIX D: CURRENT SYMMETRY

In this appendix, we describe how the coefficient symmetries, Eqs. 79–81, are obtained. These guarantee the current symmetry, Eq. 78, which must hold by the symmetry of the gramicidin channel potential of mean force. We work with the dimensionless variables described in Appendix A.

The coefficients F_i^s depend on the integrals h^s, g^s, and i^s, defined by Eqs. 114, 120, and 121, respectively. For this appendix, we define these integrals as functions of ξ and ψ as follows:

$$h^s(\xi, \psi) = \int_0^\xi \exp(\Delta\phi^s(\eta) - f^s(2\eta - 1)\psi/2)d\eta, \quad (133)$$

$$g^s(\psi) = \int_0^1 \exp(-\Delta\phi^s(\eta) + f^s(2\eta - 1)\psi/2)d\eta, \quad (134)$$

$$i^s(\psi) = \int_0^1 \exp(-\Delta\phi^s(\xi) + f^s(2\xi - 1)\psi/2)h^s(\xi, \psi)d\xi. \quad (135)$$

As a special case, note $h^s(\psi) = h^s(1, \psi)$. In the following, we make use of the symmetries of the potentials of mean force, $\Delta\phi^s(\xi) = \Delta\phi^s(1 - \xi)$, and change variables, $\xi' = 1 - \xi$ or $\eta' = 1 - \eta$, in the integrands. We find immediately

$$h^s(-\psi) = h^s(\psi), \quad (136)$$

$$g^s(-\psi) = g^s(\psi), \quad (137)$$

By the same method, it follows that

$$h^s(\xi, -\psi) = h^s(1, \psi) - h^s(1 - \xi, \psi), \quad (138)$$

which is used to obtain

$$i^s(-\psi) = g^s(\psi)h^s(\psi) - i^s(\psi). \quad (139)$$

Using these results, it is straightforward to show that the coefficients F_i^s, given by Eqs. 124–132, have the symmetries of Eqs. 79–81.

APPENDIX E: SATURATING CURRENT AT HIGH VOLTAGE

In this section, we obtain the asymptotic formula for the framework model current as $\psi_I \to \infty$, Eq. 82. Dimensionless variables are again used, see Appendix A. We must first obtain asymptotic expressions for certain integrals. The following calculations are intuitively reasonable and can be justified rigorously by use of Watson's lemma (Keener, 1988).

The integral $h^s(\xi)$ is defined by Eq. 114, where $h^s = h^s(1)$. As $\psi_I \to \infty$, the integrand becomes sharply peaked near $\eta = 0$, and it is therefore reasonable to write

$$h^s(\xi) \sim \exp(\Delta\phi^s(0))\int_0^\xi \exp(-f^s(2\eta - 1)\psi_l/2)d\eta \sim (f^s\psi_l)^{-1}\exp(f^s\psi_l/2), \quad (140)$$

where $\sim$ means $(f^s\psi_l)^{-1}exp(f^s\psi_l/2)$ is asymptotic to $h^s(\xi)$ as $\psi_I \to \infty$, in the sense of asymptotic expansions. In particular, this result holds for $h^s = h^s(1)$. The integral g^s is defined by Eq. 120. By an argument similar to the one just given, we have

$$g^s \sim (f^s\psi_l)^{-1}\exp(f^s\psi_l/2), \quad (141)$$

as $\psi_I \to \infty$. The integral i^s is defined by Eq. 121, depending on $h^s(\xi)$ whose

asymptotic behavior is given by Eq. 140. As $\psi_I \to \infty$, we have

$$i^s \sim (f^s\psi_I)^{-1}\exp(f^s\psi_I/2) \times \int_0^1 \exp(-\Delta\phi^s(\xi) + f^s(2\xi - 1)\psi_I/2)d\xi \sim (f^s\psi_I)^{-2}\exp(f^s\psi_I). \quad (142)$$

Finally, we must consider, as a special case, the combination $g^sh^s - i^s$. From the definitions, Eqs. 114, 120, and 121, we have

$$g^sh^s - i^s = \int_0^1 d\xi \int_\xi^1 d\eta \exp(\Delta\phi^s(\eta) - \Delta\phi^s(\xi) + f^s(\xi - \eta)\psi_I). \quad (143)$$

Making the substitution $\chi = \eta - \xi$, this becomes

$$g^sh^s - i^s = \int_0^1 d\chi \exp(-f^s\chi\psi_I)F(\chi), \quad (144)$$

where

$$F(\chi) = \int_0^{1-\chi} d\xi \exp(\Delta\phi^s(\xi + \chi) - \Delta\phi^s(\xi)). \quad (145)$$

The integrand of Eq. 144 is sharply peaked near $\chi = 0$, leading to

$$g^sh^s - i^s \sim (f^s\psi_I)^{-1} \quad (146)$$

as $\psi_I \to \infty$.

We are now ready to obtain the asymptotic form of the framework model current J in the limit $\psi_I \to \infty$. The exact expression for J is Eq. 74, where the terms in the denominator have the form given in Eqs. 75–77. The numerator of J grows like e^{ψ_I} as $\psi_I \to \infty$. The coefficients F_i^s in the denominator are given by Eqs. 124–132. Using the asymptotic expressions for h^s, g^s, i^s, and $g^sh^s - i^s$, we find that the only coefficient that grows as fast as e^{ψ_I} is F_0^a, whose expression is given by Eq. 130. We find

$$F_0^a \sim ae^{\psi_I - \beta\zeta}. \quad (147)$$

Then, from the expression for J, Eqs. 74–77, we obtain the result expressed by Eq. 82.

APPENDIX F: EQUILIBRIUM CONDUCTANCE

In this section, we obtain the expression, Eq. 84, for the framework model conductance at a symmetrical equilibrium. Begin by substituting the expression for the current J, Eq. 74, into formula 83 for conductance. Taking the derivative and then evaluating the resultant expression at equilibrium, find that

$$\left.\frac{dJ}{d\Psi_I}\right|_{Eq} = \frac{\beta c_I e^{\beta\Psi_I}}{t^HF^H + t^dF^d + t^aF^a|_{Eq}}. \quad (148)$$

When F^H and F^d are written out, using Eqs. 75–77 and Eqs. 124–132, they contain terms proportional to $c_Ie^{\psi_I} - c_{II}$, which vanish at equilibrium. Introducing the definitions

$$A(\psi_I) = t^Hh^H + 2t^a\cosh(f_A^d + f^H/2)\psi_I, \quad (149)$$

$$B(\psi_I) = g^d + 2a\cosh(f_B^d + f_C^d/2)\psi_I. \quad (150)$$

we can then write

$$t^HF^H + t^dF^d + t^aF^a|_{Eq} = \exp(-\beta\zeta + \psi_I/2)A(\psi_I)B(\psi_I) + [g^HA(\psi_I) + t^dh^dB(\psi_I)]c_{II} + t^dh^dg^H\exp(\beta\zeta + \psi_I/2)c_Ic_{II}. \quad (151)$$

In the case of a symmetrical equilibrium, $c_I = c_{II} = c$ and $\psi_I = 0$, the denominator can be written in the factored form

$$t^HF^H + t^dF^d + t^aF^a|_{Eq} = [A(0)e^{-\beta\psi_I} + t^dh_0^dc][B(0) + g_0^He^{\beta\zeta}c]. \quad (152)$$

Note that $B(0) = g^d + 2a$, where g^d is defined by Eq. 120 and a by Eq. 65. When g^d is written in dimensional form, $g^d + 2a = g_1^d$, as defined by Eq. 88. Inserting the result of Eq. 152 into Eq. 148 then leads to Eq. 84.

Mark F. Schumaker thanks Ann Schumaker for carefully editing the manuscript. He is supported by grant MCB 9630475 from the National Science Foundation.

Régis Pomès is supported in part by the US Department of Energy through the Los Alamos National Laboratory-Directed Research and Development grant for bioremediation.

Benoît Roux is supported by the Medical Research Council of Canada.

REFERENCES

Akeson, M., and D. W. Deamer. 1991. Proton conduction by the gramicidin water wire. *Biophys. J.* 60:101–109.

Andersen, O. S. 1983. Ion movement through gramicidin A channels. Interfacial polarization effects on single-channel current measurements. *Biophys. J.* 41:135–146.

Chandrasekhar, S. 1943. Stochastic problems in physics and astronomy. *Rev. Mod. Phys.* 15:1–89.

Chen, D., J. Lear, and R. S. Eisenberg. 1997. Permeation through an open channel: Poisson–Nernst–Planck theory of a synthetic ion channel. *Biophys. J.* 72:97–116.

Cooper, K. E., P. Y. Gates, and R. S. Eisenberg. 1988. Diffusion theory and discrete rate constants in ion permeation. *J. Membr. Biol.* 106: 95–105.

Cooper, K., E. Jakobsson, and P. Wolynes. 1985. The theory of ion transport through membrane channels. *Prog. Biophys. Molec. Biol.* 46: 51–96.

Dani, J. A., and D. G. Levitt. 1990. Diffusion and kinetic approaches to describe permeation in ionic channels. *J. Theor. Biol.* 146:289–301.

Decker, E. R., and D. G. Levitt. 1988. Use of weak acids to determine the bulk diffusion limitation of H^+ ion conductance through the gramicidin channel. *Biophys. J.* 53:25–32.

Dieckmann, G. R., J. D. Lear, Q. Zhong, M. L. Klein, W. F. DeGrado, and K. A. Sharp. 1999. Exploration of the structural features defining the conduction properties of a synthetic ion channel. *Biophys. J.* 76: 618–630.

Eisenman, G., B. Enos, J. Hagglund, and J. Sandblom. 1980. Gramicidin as an example of a single-filing ionic channel. *Ann. NY Acad. Sci.* 339: 8–20.

Hille, B. 1992. Ionic Channels of Excitable Membranes, 2nd ed. Sinauer Assoc. Inc., Sunderland, MA.

Hille, B., and W. Schwarz. 1978. Potassium channels as multi-ion single-file pores. *J. Gen. Physiol.* 72:409–442.

Jackson, J. D. 1975. Classical Electrodynamics, 2nd ed. John Wiley & Sons, New York.

Jakobsson, E., and S. W. Chiu. 1987. Stochastic theory of ion movement in channels with single-ion occupancy: application to sodium permeation of gramicidin channels. *Biophys. J.* 52:33–45.

Jordan, P. C., R. J. Bacquet, J. A. McCammon, and P. Tran. 1989. How electrolyte shielding influences the membrane potential in transmembrane ion channels. *Biophys. J.* 55:1041–1052.

Karlin, S., and H. M. Taylor. 1981. A Second Course in Stochastic Processes. Academic Press, New York. 157–191.

Keener, J. P. 1988. Principles of Applied Mathematics. Addison-Wesley, Redwood City, CA. 434–437.

Kurnikova, M. G., R. D. Coalson, P. Graf, and A. Nitzan. 1999. A lattice relaxation algorithm for three dimensional Poisson–Nernst–Planck theory with application to ion transport through the gramicidin A channel. *Biophys. J.* 76:642–656.

Läuger, P. 1973. Ion transport through pores: a rate theory analysis. *Biochim. Biophys. Acta.* 311:423–441.

Levitt, D. G. 1986. Interpretation of biological ion channel flux data: reaction rate versus continuum theory. *Annu. Rev. Biophys. Biophys. Chem.* 15:29–57.

McGill, P., and M. F. Schumaker. 1996. Boundary conditions for single-ion diffusion. *Biophys. J.* 71:1723–1742.

Phillips, L. R., C. D. Cole, R. J. Hendershot, M. Cotten, T. A. Cross, and D. D. Busath. 1999. Noncontact dipole effects on channel permeation. III. Anomalous proton conductance effects in gramicidin. *Biophys. J.* 77:2492–2501.

Pomès, R., and B. Roux. 1996. Structure and dynamics of a proton wire: a theoretical study of H^+ translocation along the single-file chain in the gramicidin A channel. *Biophys. J.* 71:19–39.

Pomès, R., and B. Roux. 1997. Free energy profiles governing H^+ conductance in proton wires. *Biophys. J.* 72:A246.

Press, W. H., S. A. Teukolsky, W. T. Vetterling, and B. P. Flannery. 1992. Numerical Recipes in Fortran. 2nd ed. Cambridge University Press, New York. 272–273.

Robinson, R. A., and H. Stokes. 1965. Electrolyte Solutions. Butterworths, London. 45–48.

Roux, B., and M. Karplus. 1993. Ion transport in the gramicidin channel: free energy of the solvated right-hand dimer in a model membrane. *J. Am. Chem. Soc.* 115:3250–3262.

Roux, B. 1997. Influence of the membrane potential on the free energy of an intrinsic protein. *Biophys. J.* 73:2980–2989.

Roux, B. 1999. Statistical mechanical equilibrium theory of selective ion channels. *Biophys. J.* 77:139–153.

Schumaker, M. F., and R. MacKinnon. 1990. A simple model for multi-ion permeation. *Biophys. J.* 58:975–984.

Schumaker, M. F., R. Pomès, and B. Roux. 2000. A combined molecular dynamics and diffusion model of single proton conductance through gramicidin. *Biophys. J.* 79:2840–2857.

Zauderer, E. 1989. Partial Differential Equations of Applied Mathematics. 2nd ed. Wiley-Interscience, New York. 1–45.